Polymetallaynes and molecular metallaynes containing platinum, mercury and gold for optoelectronic and magnetic applications

Chen Zhang, Linli Xu, and Wai-Yeung Wong*

Department of Applied Biology and Chemical Technology, The Hong Kong Polytechnic University, Hung Hom, Hong Kong, China

What is the most favorite and original chemistry developed in your research group?

Chemistry plays a key role in providing solutions to many of the challenges facing the world today. In particular, an understanding of chemistry is essential as the basis for medicine and public health, in addressing challenges such as global climate change, in providing sustainable sources of clean energy, and in maintaining the environment for the well-being of people. We aim at the cutting-edge research areas of photofunctional metal-organic molecules and polymers for optoelectronic and energy-related applications. Photofunctional molecular materials are considered as versatile materials for energy interconversions and optoelectronic/photonic applications, including electrical energy generation in organic solar cells (OSCs) and light generation in organic light-emitting diodes (OLEDs), as they offer a low cost, light weight and simple option for device fabrication. We have developed new synthetic methods to produce technologically useful materials (e.g. metallopolymers and metallophosphors) with specific functional roles. Such research clearly presents a promising way out of the worldwide energy problem.

What is the most important personality for scientific research?

Although there is no guarantee of success and practical gains in doing research, it is my belief that our efforts will get harvest if we work hard and do not give up. Patience, diligence, perseverence and confidence are the prerequisites for the successful research study. Besides, there are many good research opportunities in the Greater Bay Area and the Mainland by collaborating with the top researchers there in various joint projects, which would create more impact cases for the betterment of our society.

How do you get into this specific field? Could you please share some experiences with our readers?

Global energy consumption is depleting non-renewable fossil fuels at a staggering rate. Mankind's life quality depends on the development of renewable energy sources. As such, our research is dedicated to advancing technologies in energy conversion and translating light into electricity and electricity into light, hence contributing to the sustainability of human life on earth. Our main focus is to develop molecular materials for fabricating OSCs and OLEDs. These developments are complementary in that solar devices produce energy, and light-emitting devices save energy.

How do you supervise your students?

I was deeply inspired by the passion of my former supervisors for research when I did my PhD and postdoctoral studies. Their ability to captivate me with the inherently intriguing essence of science and to share with me their passion for the discipline was particularly rewarding for me. Certain qualities I developed, such as an analytic mind and creative thinking, are the key factors that help me handle my job well nowadays. I hope that young talents will make full use of the word "Chem-is-try" to try more in chemical research and explore new interesting science topics. Besides, students can realize the magic of scientific research which probes them to achieve more.

Professor Wai-Yeung Wong obtained his B.Sc.(Hons.) and Ph.D. degrees from the University of Hong Kong. After postdoctoral works at Texas A&M University (with Prof. F.A. Cotton) and the University of Cambridge (with Profs. The Lord Lewis and P.R. Raithby), he joined Hong Kong Baptist University from 1998 to 2016 and now works at the Hong Kong Polytechnic University as the Dean of Faculty of Science and Chair Professor of Chemical Technology. He is also the President of the Hong Kong Chemical Society. Among his awards are the RSC Chemistry of the Transition Metals Award, FACS Distinguished Young Chemist Award, State Natural Science Award from China and RGC Senior Research Fellow Award. His research focusses on synthetic inorganic/organometallic chemistry, aiming at developing photofunctional metal-organic molecules and polymers for optoelectronic and energy-related applications.

Keywords

Polymetallayne | Molecular metallayne | Metallated graphyne | Platinum | Mercury | Gold

Comprehensive Summary

Polymetallaynes are a promising branch of metallopolymers, in which the introduction of metal building blocks to organic conjugated backbones leads to their unique skeletons and versatile properties. Notably, the chemical structures, geometric configurations and functional properties in these organometallic systems can be adjusted flexibly by the appropriate selection of metal centers, auxiliary ligands, or bridging spacers. In recent years, both one-dimensional and two-dimensional polymetallaynes have attracted considerable attention owing to their excellent electronic, optical and magnetic properties. Furthermore, the studies on molecular metallaynes provide substantial insights for the exploration of the structure-property-activity relationships in these organometallic acetylide-containing systems. The recent research progress of polymeric and molecular metallaynes containing platinum, mercury and gold is discussed in this article. A series of functional properties have been realized in these acetylide-containing compounds by the rational structural design and refined synthetic strategies, leading to their emerging applications including energy conversion, nonlinear

optics, data storage and memory, as well as chemo/biosensing.

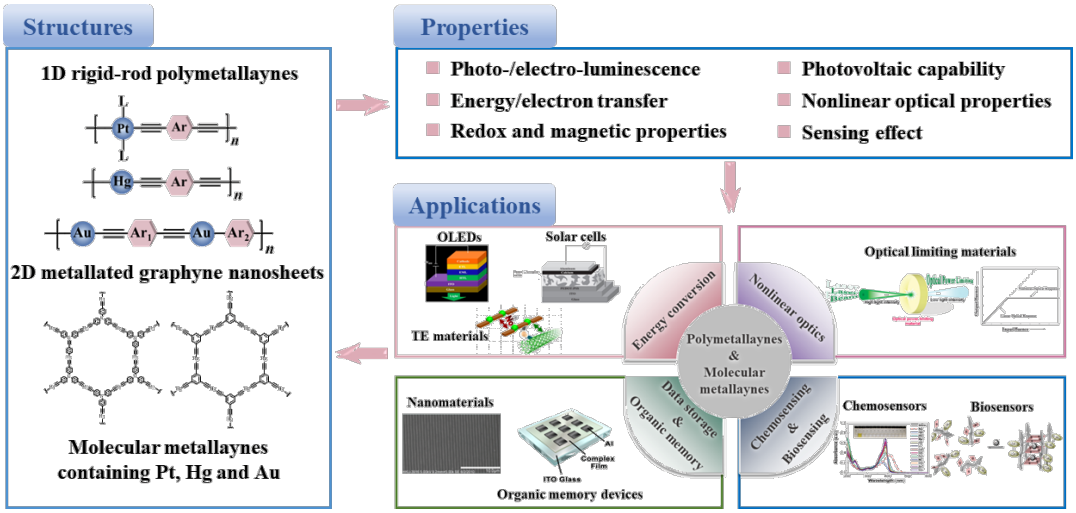

Contents

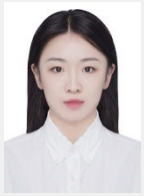

Chen Zhang obtained her B.Sc. and M.Sc. degrees from Shaanxi Normal University. She is currently a PhD student at the Hong Kong Polytechnic University under the supervision of Prof. Wai-Yeung Wong. Her research interests include the design, synthesis and functional applications of metallated graphynes.

Dr Linli Xu is a research assistant professor in the Department of Applied Biology and Chemical Technology at the Hong Kong Polytechnic University. She obtained her PhD degree in 2010 from Guangzhou Institute of Chemistry, Chinese Academy of Sciences (CAS), in Polymer Chemistry and Physics. She was a postdoctoral fellow at Technical Institute of Physics and Chemistry (IPC), CAS, from 2010 to 2012. Then she is an assistant researcher at IPC, CAS, from 2012 to 2017.

1. Introduction

Conjugated polymers are a representative type of organic materials with extensive π-conjugated electronic structure, demonstrating excellent photophysical and electrochemical properties.[1,2] Metallopolymers prepared by inserting metal blocks into the conjugated skeletons display different characteristics from pristine organic conjugated systems, such as the enhanced reactivity, enriched optoelectronic and magnetic properties.[3] Especially, the presence of heavy metal ions in conjugated frameworks significantly contributes to the spin-orbit coupling (SOC) and results in the promotion of intersystem crossing (ISC) from the singlet to the triplet states, thereby increasing the population of triplet excited states. Hence, both fluorescent and phosphorescent emissions can be realized in such organometallic systems. Besides, the metal centers can be regarded as electron-rich units compared to their adjacent organic ligands, which allows the energy transfer along the conjugated skeletons.[4]

Transition metal acetylide polymers or polymetallaynes with direct metal-carbon *σ*-bonds have drawn great research interest owing to their intriguing properties and multiple application prospects.[4,5] First examples of Pt(II)-containing acetylide oligomers and polymers with tertiary phosphine ligands were reported by Hagihara in 1970s.[6,7] Thereafter, numerous rigid-rod polymetallaynes with various metal centers and organic ligands have been reported, leading to their rich applications. The desired properties can be orchestrated by the elaborate design and appropriate structural regulation of these polymetallaynes, which involve the exploitation of metal centers, auxiliary ligands and organic bridging spacers. Furthermore, the vast body of synthetic methodologies provides variable and low-cost approaches for the fabrication of polymetallaynes.

Our research group is committed to the development of polymeric and molecular metallaynes and the exploration of structure-property-activity relationships in different organometallic systems, thereby realizing a series of emerging applications, including organic light-emitting diodes (OLEDs), organic solar cells (OSCs), organic thermoelectric (OTE) devices, optical power limiting (OPL), data storage devices and sensors. It is worth noting that two-dimensional (2D) free-standing mercurated graphyne nanosheets have been reported for the first time by our group, which demonstrated remarkable nonlinear optical (NLO) responses.[8] The creation of these novel 2D metallated graphynes is of great significance to the development of organometallic material field, contributing to the further exploration of their functional properties and potential applications. In this article, a series of fundamental studies and the application-oriented explorations of organometallic acetylide-containing systems will be emphasized. The structure-property-activity relationships in such systems are expatiated to provide enlightening paradigms for the subsequent research in this field. The structures and syntheses of polymetallaynes and molecular metallaynes containing platinum, mercury

and gold will be introduced first, accompanied by the representative methods to tune their properties. A series of applications achieved by the fine-tuning of structures and properties in the above systems will then be described in sequence. Finally, the challenges and future prospects in this field will be presented in the corresponding sections.

2. Structures and properties

2.1. Polyplatinaynes

As illustrated in Figure 1a, polyplatinaynes [–$PtL_2C{\equiv}CArC{\equiv}C–]_n$ are comprised of bridging spacers Ar and Pt(II) building blocks containing auxiliary coordinated ligands L (L = PBu_3, PEt_3, etc.). Generally, polyplatinaynes are synthesized via classical dehydrohalogenation reaction between Pt(II) halide complexes [PtL_2Cl_2] and diethynylarylene ligands [HC≡CArC≡CH] (Figure 1b), in which CuI acts as the catalyst whilst amine serves as the acid acceptor and reaction solvent.[5] The above polymerization can proceed at ambient temperature smoothly and generally afford air-stable polymeric products soluble in organic solvents. The chain length and the degree of solubility in such organometallic systems can be regulated by the appropriate selection of metal centers, organic spacers and auxiliary ligands. This favorable feature is beneficial to solving the poor solubility encountered in classical purely organic polymers, thereby facilitating the preparation of polymer films for optoelectronic measurements.

The inclusion of heavy Pt(II) ions into the conjugated backbone effectively increases the ISC rate from the singlet to triplet states due to the enhanced SOC effect, enabling the spin-forbidden triplet emission to be observed in these metal polyyne systems. Besides, in comparison with the pure organic conjugated polymers, the π-conjugation interaction between Pt(II) centers and the bridging spacers in polyplatinaynes has significant influence on the distribution of delocalized electrons along the organometallic skeleton, thereby changing the optical and electronic properties of polyplatinaynes. Therefore, the regulation of organic spacers in these polyplatinaynes is an effective approach to tune their lowest singlet (S_1) and triplet (T_1) energy levels, energy gap (E_g) and color.[9]

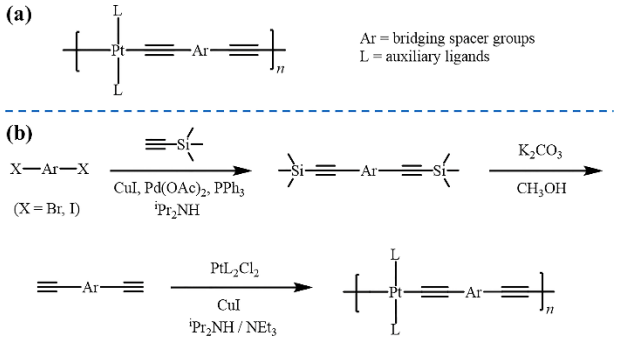

Figure 1 (a) The general structure of polyplatinaynes. (b) The synthesis of polyplatinaynes by copper-catalyzed dehydrohalogenation reaction.

The optical properties were successfully tuned in Pt(II)-based polyynes by extending the effective conjugation length of the organic spacers. For instance, the increased phenyl ring number in **1b** results in its red-shifted phosphorescence and lowered T_1 energy level (2.26 eV) compared to **1a** (2.38 eV).[10] Similarly, the T_1 energy bands of **2a**-**2c** are 2.05, 1.67 and 1.53 eV, respectively, with the obvious energy drop due to the inclusion of more thiophene rings into their spacers, whilst the red-shifted triplet emissions in these polymers indicate that their triplet excited states are extended over several thiophene units.[11,12]

Furthermore, the introduction of fused ring spacers leads to the decrease in E_g of these metallopolyynes. Polymers **3** and **4** with electron-rich naphthalene and anthracene ligands, respectively, display bathochromically-shifted luminescence compared

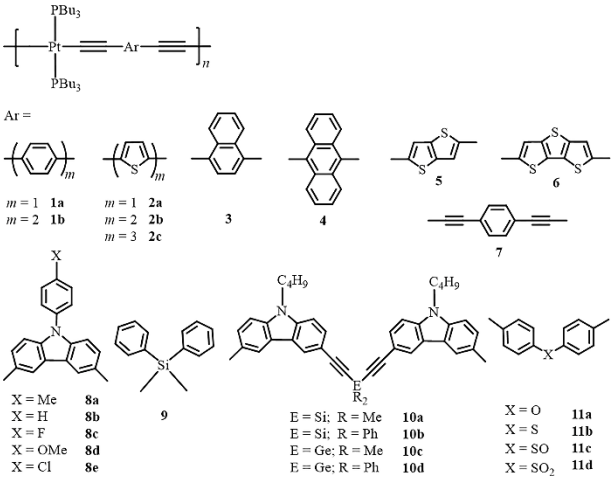

with **1** due to their extended π-conjugated linkers and enhanced π-electron delocalization along the polymeric skeletons.[13] Although **5** and **6** possess planar fused ring spacers, their energy levels of S_1 and T_1 are both higher than those of **2b** and **2c** containing non-fused ring spacers with the same number of thiophene rings.[14] Thus, the effectiveness of conjugation and the number of sulfur atoms in the oligothiophene units contribute jointly to the electronic energy states in such fused ring and non-fused ring-based metallopolyynes. Compared with their non-fused ring analogues, the increase of sulfur atom number in the fused ring-containing metallopolyynes weakens the conjugation of double bonds, resulting in their relatively wider energy gaps. Besides, the effective conjugation length can also be tuned by altering the number of alkyne bonds in polyplatinaynes. Compared with **1a**, polymer **7** displays red-shifted phosphorescence since there is a double number of triple bonds in polymer **7**.[15]

According to the energy gap law of polyplatinaynes, the decrease of triplet energy leads to the exponential increase of non-radiative decay rate of the triplet states.[16] As a consequence, the introduction of π-conjugation interrupters into the spacers allows the metallopolyynes to possess high triplet energy states, resulting in the reduced non-radiative decay and more effective phosphorescence emission.[17,18] Polymers **8a**-**8e** are made with the nitrogen at the 9-position of the 3,6-carbazole unit as conjugation interrupter,[19] which demonstrate relatively high T_1 energy states at around 2.68 eV, despite the variation in their 9-aryl group substituents.

Group 14 Si or Ge-based linkers and group 16 chalcogen atoms are also effective conjugation interrupters. The incorporation of $SiPh_2$ unit into polymer **9** results in a blue-shifted phosphorescence band compared to the polyplatinaynes with other spacers.[20] Besides, **9** exhibited negligible fluorescent emission but intense unstructured triplet emission at 508 nm at low temperature. The E_g of **9** (3.7 eV) is much higher than those of **1a** (E_g = 2.98 eV) and **2a** (E_g = 2.85 eV), while the T_1 energy state of **9** (2.44 eV) is blue-shifted by 0.06 eV and 0.38 eV in comparison to **1a** and **2a**, respectively. Similarly, triplet emission with fast phosphorescence decay rate can be achieved by introducing sp^3 heavier Ge-based units into such organometallic systems.[21] In **10a**-**10d** with diethynylcarbazole units, the variation in ER_2 linkers results in distinct changes in their phosphorescence emission efficiency, following the general orders: $GeR_2 > SiR_2$ (R = Me or Ph), and $EMe_2 > EPh_2$ (E = Si or Ge).[22]

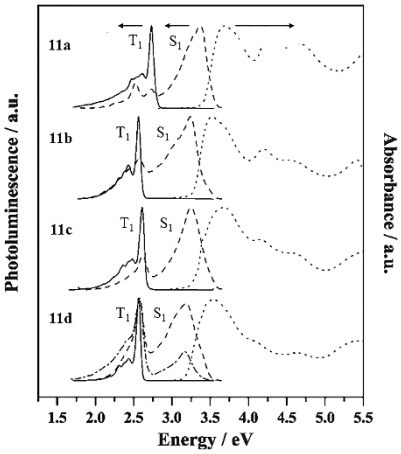

Figure 2 (a) The absorption and photoluminescence (PL) spectra of **11a-11d**. The absorption spectra (dotted lines) were measured at 290 K. The PL spectra were recorded at 290 K (dashed lines, in CH_2Cl_2) and 20 K (solid lines, as thin films). Reproduced with permission from ref. 23. Copyright 2006, Wiley-VCH.

Polymers **11a**-**11d** containing non-conjugated group 16 heteroatoms were determined to possess high T_1 energy states, in which the accessibility of $^3\pi$-π^* excited states was promoted, enabling the spin-forbidden phosphorescence to be observed at ambient temperature (Figure 2).[23] The phosphorescence bands of **11a**-**11d** with different chalcogenide linkers are blue-shifted in comparison to the biphenyl-based **1b**, among which **11a** with the diphenyl ether unit gives the T_1 energy level of 2.73 eV with the largest extent of the blue shift (0.47 eV).

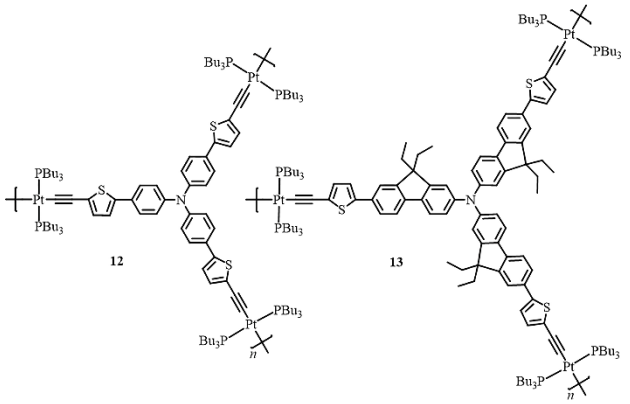

The construction of metallopolyynes with higher dimensionality provides an attractive strategy to improve the isotropic charge transport as well as the optical properties in organometallic materials. Apart from the rigid-rod polyplatinaynes discussed above, **12** and **13** with pseudo-three-dimensional (pseudo-3D) structures have been developed by our group, in which the triphenylamine units present non-planar propeller shape due to the steric interactions between the organic spacers, resulting in an intermediate situation between the 2D and 3D conjugated systems.[24] Notably, **13** with extended π-conjugation segments displays more enhanced light-harvesting and charge-transport abilities in comparison to its 1D counterpart. Under the same testing conditions, the thin film of **13** gave an impressive absorption coefficient of 1.59×10^5 cm^{-1} at 430 nm, while that of **12** was measured to be 1.05×10^5 cm^{-1} at 413 nm. **12** and **13** showed relatively high E_g of 2.68 eV and 2.59 eV, respectively. Besides, the organic field-effect transistor (OFET) devices based on **12** and **13** demonstrated typical *p*-channel output characteristics with the average hole mobilities of 7.86×10^{-5} cm^2 V^{-1} s^{-1} and 2.77×10^{-5} cm^2 V^{-1} s^{-1}, respectively, which are both superior to that of their linear counterpart. These pseudo-3D metallopolyynes have been successfully utilized in the fabrication of high-efficiency solar cells, proving their great application potentials in energy conversion.

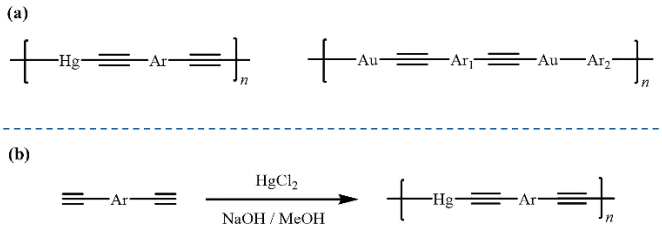

Figure 3 (a) The general structures of Hg(II)- and Au(I)-containing polymetallaynes. (b) The synthesis of Hg(II)-based polymetallaynes by base-catalyzed mercuration reaction.

2.2. Hg(II)- and Au(I)-containing polymetallaynes

Transition metal elements from the neighboring groups of Pt have also been investigated as active centers for the construction of polymetallic aryleneethynylenes.[25] Similar to the polyplatinayne systems aforementioned, SOC is effectively facilitated in the presence of these heavy metals in conjugated backbones, leading to the promoted ISC process from the S_1 to the T_1 states. The general skeletons of Hg(II)- and Au(I)-containing polyynes are depicted in Figure 3a. Hg is a unique element among the group 12 metal species due to the formation of stable Hg(II) ion, which tends to present a coordination number of two and linear geometry for the preparation of rigid-rod polymetallaynes. However, linear Hg(II) polyynes often suffer from the unsatisfactory solubility, hindering their practical applications to a large extent. To circumvent this issue, our group designed and synthesized a series of Hg(II)-containing polyynes **14**-**17** with various organic spacers.[10,26,27] The Hg(II) alkynyl complexes and polymers can be prepared by base-catalyzed dehydrohalogenation protocol between Hg(II) halide precursors and active terminal alkynes. This reaction can be achieved with good yield at room temperature, providing a convenient method for the preparation of Hg(II)-containing polymetallaynes (Figure 3b). Specifically, the mercuration of the corresponding ligands with $HgCl_2$ can be realized with the presence of methanolic NaOH. The air-stable polymers **14**-**17** can be precipitated from the respective homogeneous solution in the synthetic processes. It is worth noting that the introduction of long alkyl chains in **14a**-**14c, 16** and **17** endows them with good solubilities in common organic solvents, whereas only the fractions of **15** with lower molecular weight can be dissolved in organic solvents. The Hg(II)-induced $^3\pi$-π^* phosphorescence can be observed in most cases of these polymetallaynes. Besides, the broadening emissions in the films of such Hg(II)-containing polyynes indicates the weak intermolecular Hg(II)···Hg(II) short contacts in the solid form.

14a-**14c** are the first examples of soluble Hg(II) polyynes with 9,9-dialkylfluorene spacers, displaying similar absorption bands in the near-UV region. Notably, all the three Hg(II) polyynes give large optical bandgaps in the range of 3.31-3.32 eV due to the introduction of Hg(II) ions, whereas the C-9 substituents on the fluorene units exert a negligible influence on the absorption energy and E_g in these polymers. The phosphorescence spectra of these Hg(II)-containing polyynes show a strong temperature dependence (Figure 4), and their S_1-T_1 crossover efficiency follows the order: **14c** > **14b** > **14a**. Besides, the decomposition temperatures of **14a**-**14c** increase with the decrease of chain length in their substituent groups. Polymers **15** and **1b** with different metal centers exhibit distinct optical bandgaps (3.27 and 3.10 eV for **15** and **1b**, respectively), whilst their energy gaps between S_0 and T_1 states are measured to be 2.26 and 2.36 eV, respectively. For polymers **16** and **17**, the different positions of the substituents in

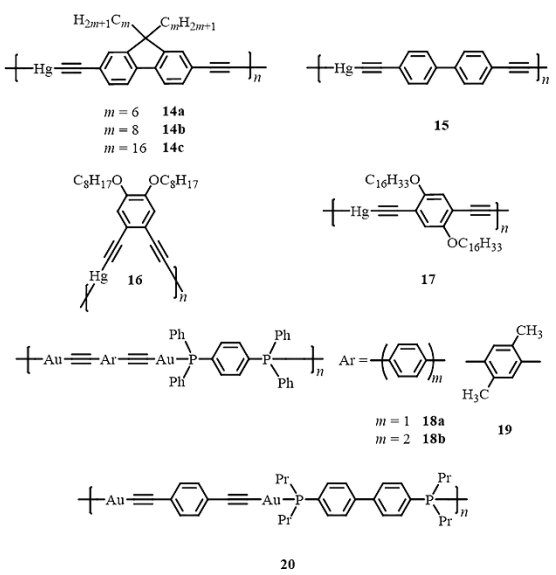

aromatic spacers lead to similar emission peaks but different emission intensities in dichloromethane at ambient temperature. Besides, **16** featured more efficient phosphorescence than that of **17** at 77 K. From the thermogravimetric analysis, the decomposition temperatures of **16** and **17** are 306 °C and 232 °C, respectively, indicating the better thermostability of **16** as compared to **17**.

Polymeric Au(I)-acetylides with diphosphine or bis-(isocyanide) ligands were firstly synthesized by Puddephatt's group via the reaction between PPN ($Au(acac)_2$) and diethynylarenes, which could only be investigated in the solid state due to their insolubility in organic solvents.[28] The bathochromic shifts in the emission spectra were concomitant with the structures of Au(I)-containing compounds changed from the mononuclear, binuclear to polynuclear. The Au(I)-containing polyynes **18**-**20** showed broad and weak emissions at around 600 nm, proving the interchain Au(I)···Au(I) bonding interactions in the solid state.

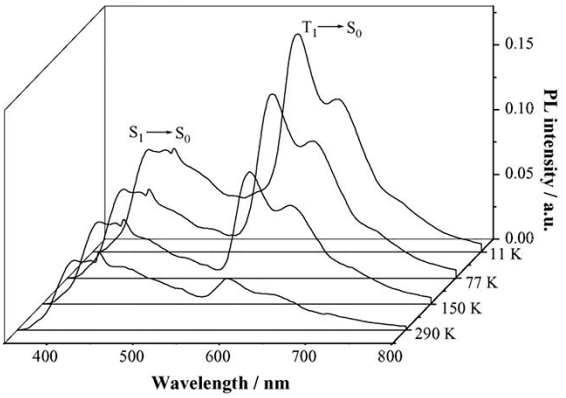

Figure 4 Temperature dependence of the PL spectra in **14c**. Reproduced with permission from ref. 5. Copyright 2006, Elsevier B.V.

Two novel mercurated acetylenic 2D nanosheets **21** and **22** were fabricated for the first time by our group through interface-assisted bottom-up strategy, demonstrating layered molecular arrangement, promoted π-conjugation effect, adjustable thickness, as well as low cytotoxicity.[8] As illustrated in Figure 5, **21** and **22** both demonstrated outstanding nonlinear saturable absorption (SA) properties at both 532 nm and 1064 nm, leading to their promising applications in the fabrication of optoelectronic devices. The excellent passively Q-switched (PQS) performance has been achieved by utilizing these nanosheets as the saturable absorbers, which will be discussed specially in the corresponding sections.

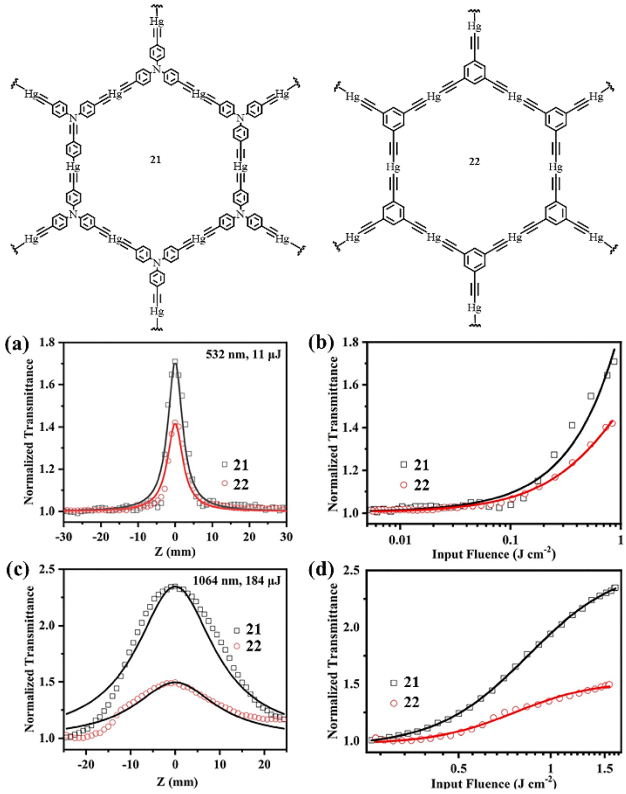

Figure 5 NLO properties of mercurated graphyne nanosheets **21** and **22**. Open-aperture Z-scan data and theoretically fitted curves (solid lines) at (a) 532 nm with an input energy of 11 μJ and (c) 1064 nm with an input energy of 184 μJ. Theoretically fitted plots of normalized transmittance versus incident intensity at (b) 532 nm with an input energy of 11 μJ and (d) 1064 nm with an input energy of 184 μJ. Reproduced with permission from ref. 8. Copyright 2021, Wiley-VCH.

2.3. Heterobimetallic acetylide-containing polymers

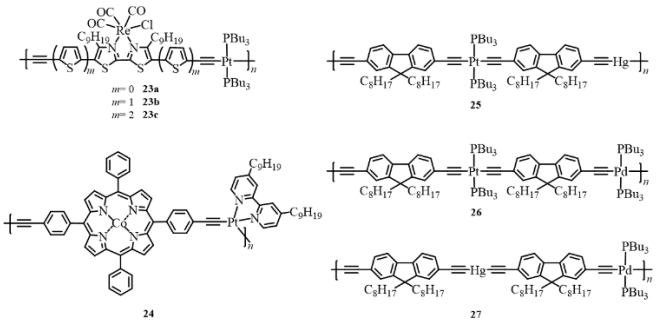

The incorporation of two metal ions into a single organometallic backbone possesses a great appeal, which enables the functional properties to be tuned by the synergistic effect between the different metal centers in such bimetallic conjugated systems. In particular, the paired nitrogen atoms in bithiazole segments can be utilized as suitable sites for the coordination between metal ions and organic moieties. Compared to their counterparts without $Re(CO)_3Cl$ groups, obvious red shifts were observed in the absorption spectra solution-processable heterobimetallic polymers **23a**-**23c**, owing to the electron-withdrawing effect of the Re(I) blocks towards the bithiazole cores.[29] The coordination between polymeric backbone and $Re(CO)_3Cl$ units leads to a reduction in the E_g of these polymers, while the E_g values of **23a**-**23c** decrease from 2.18 eV to 1.89 eV with the inclusion of more thiophene rings into the conjugated backbones. A heterobimetallic polymer **24** containing Pt(II) and Co(II) moieties was synthesized, in which the Co(II) ion coordinated with the four central N atoms in the porphyrin unit.[30] The preparation of CoPt nanoparticles

(NPs) without any post annealing operation was achieved by using **24** as the precursor, indicating the application prospect of **24** in data storage. It is worth noting that heterobimetallic polyynes **25**-**27** have been demonstrated to possess different NLO performance, leading to their important research value for the construction of OPL materials, which will be introduced in detail in the following sections.[31]

2.4. Molecular metallaynes containing Pt(II), Hg(II) and Au(I)

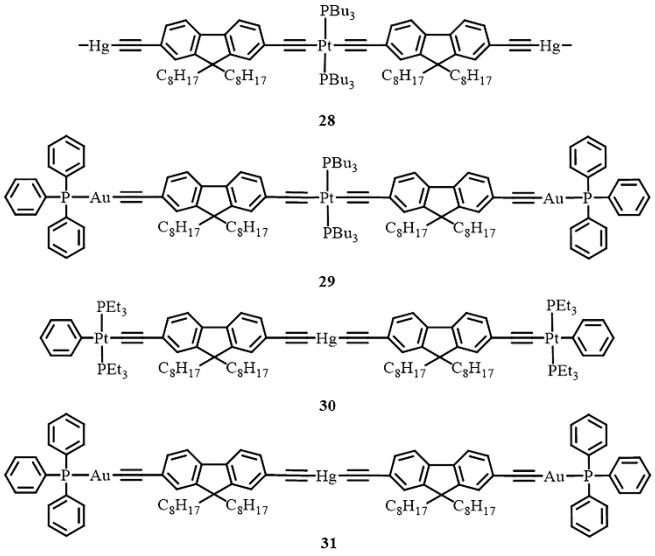

28

29

30

31

Apart from the metallopolyynes, representative molecular metallaynes containing Pt(II), Hg(II) and Au(I) are also discussed in this article. The research on molecular metallaynes greatly contributes to the in-depth exploration of the structure-function relationships in organometallic systems, whilst these small molecules have been developing rapidly in recent years and have achieved widespread applications in related fields. For instance, solution-processable heterometallic complexes **28**-**31** were prepared for the investigation of their OPL properties.[31]From the research results, complex **28** with the Pt(II) ion at the central position demonstrated superior OPL effect as compared to **30** with the Hg(II) center, while the latter showed no triplet emission at room temperature. Although the introduction of Hg(II) and Au(I) ions may lead to an adverse impact on the SOC induced by Pt(II) center, **28** and **29** both exhibited comparable OPL capabilities to their congener containing only Pt(II) center. Collectively, these results illustrate that the central metal ions play a decisive role in the OPL performance of such metal complexes.

3. Applications

The unique skeleton of metallated acetylenic polymers containing both metal centers and organic moieties endows them with extensive π-conjugated framework and tunable optoelectronic properties, whilst the targeted structures of these metallated polyynes can be obtained conveniently owing to their flexible synthetic strategies and moderate preparation conditions. These integrated virtues enable such metallic conjugated systems to possess irreplaceable prospects in the fabrication of multifunctional devices, leading to their consequential applications in diverse fields. The representative applications of metal acetylide polymers and their small molecular analogues are elucidated sequentially in the following sections, including energy conversion, nonlinear optics, data storage and organic memory, as well as chemo/biosensing.

3.1. Energy conversion

Energy crisis has become a worldwide issue at the expense of the continuous development of human society. The exploitation of renewable energy and technologies for energy conversion thus attracts an on-going attention in various scientific disciplines. Organometallic compounds have been successfully deployed to construct OLEDs, solar cells and OTE devices for the transformations of light into electricity, electricity into light and heat into electricity, respectively, illustrating the great applicability of metallated acetylenic systems in different energy interconversions.

3.1.1. OLEDs

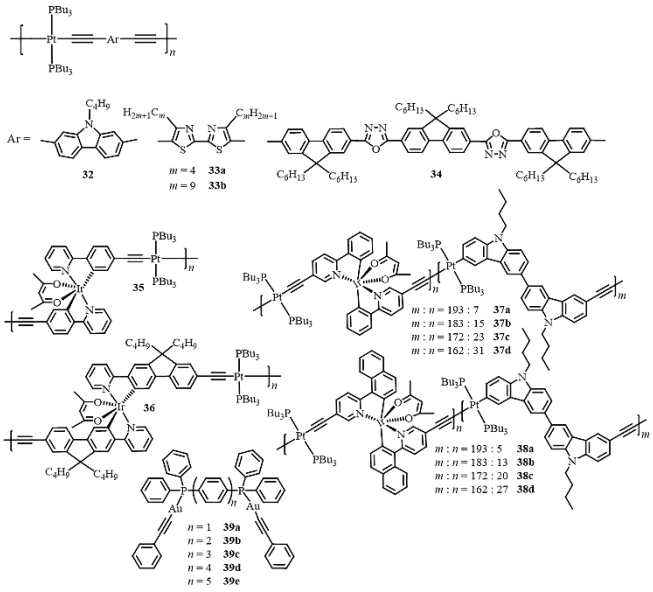

32 **33a** **33b** **34** **35** **36** **37a** **37b** **37c** **37d** **38a** **38b** **38c** **38d** **39a** **39b** **39c** **39d** **39e**

The SOC effect induced by heavy metal centers contributes to the mixed triplet and singlet excited states in the metallopolyynes, resulting in the effective triplet emission for OLED applications. Polyplatinayne **32** with 9-butylcarbazole-2,7-diyl spacer exhibited strong phosphorescence at 527 nm at room temperature with high phosphorescence efficiency of 2.5%.[32] Besides, the E_g of **32** is 2.95 eV, which is lower than that of its 3,6-disubstituted counterpart. The general structure of polymer light emitting diode (PLED) device is demonstrated in Figure 7a. The PLED based on **32** showed a strong greenish yellow electrophosphorescence, and their electroluminescence (EL) spectra gave a prominent band peaking at 528 nm together with a shoulder at 568 nm (Figure 6). The efficiency of devices increases as a function of doping concentration when the doping concentration is below 5 wt.-%, which significantly decreases due to the concentration quenching effect at the higher concentration above 5 wt.-% (Figure 7b-d). The maximum current efficiency (η_L) can reach 4.7 cd A^{-1} at the doping concentration of 5 wt.-% with the corresponding external quantum efficiency (η_{ext}) of 1.5% and power efficiency (η_p) of 1.6 lm W^{-1}. This report is the first example of metallopolyyne-based PLEDs with pure triplet emission under electrical excitation, revealing the significant potentials of metallated polyynes in PLED applications.

Polymers **33a** and **33b** containing electron-deficient bithiazole spacers possess low optical bandgaps of 2.4 eV, deriving from their particular donor-acceptor (D-A) structures.[33] There was no phosphorescence found in **33a** and **33b** at both ambient and low temperatures. Apart from the excellent thermal stability of **33a** and **33b** over 340 °C, their good solubility in common organic solvents is also observed, which makes these solution-processable polymers suitable for the construction of devices. The multi-layer PLED based on **33b** exhibited a prominent EL peaking at around 500 nm accompanied by a shoulder (522 nm) with the Commission Internationale de L'Eclairage (CIE) coordinates of (0.26, 0.58). The maximum η_L of the non-optimized PLED is confirmed to be

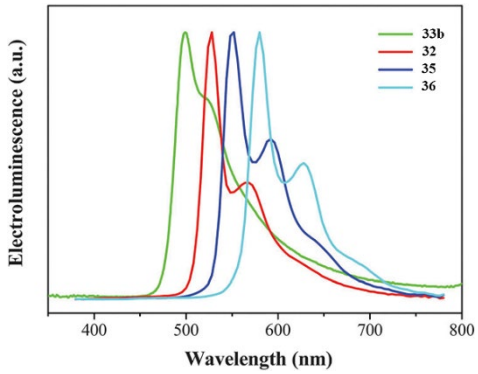

Figure 6 The electroluminescence (EL) spectra of the PLED devices fabricated by **33b**, **32**, **35**, **36**. Reproduced with permission from ref. 3. Copyright 2016, The Royal Society of Chemistry.

0.11 cd A^{-1} and further studies are still required.

In 2010, a series of polyplatinaynes with two-photon absorption properties were reported, among which **34** was employed to fabricate electrophosphorescent PLED.[34] With the doping content of **34** at 1 wt.-%, the η_{ext} and η_L of the as-prepared device were measured to be 0.15% and 0.58 cd A^{-1}, respectively. It is worth noting that **34** can realize nearly white luminescence under appropriate conditions, thereby providing a promising platform for the construction of white polymer light-emitting diodes (WPLEDs).

The incorporation of heavy Ir(III) ion with a large SOC constant into conjugated polymers provides these systems with more enhanced triplet state characters, leading to the promotion of luminescence performance by harnessing the singlet or triplet excited state of Ir chromophores. Polymers **35** and **36** are the first examples of phosphorescent bimetallic polyynes containing both Ir(III) and Pt(II) centers, which exhibit synergistic effect in governing the photophysical characteristics of organometallic compounds.[35] These polymers generated yellow or orange phosphorescence upon light irradiation, while their emission spectra showed obvious vibronic progressions. These results indicate that the phosphorescence is mainly derived from the ligand-centered (LC) π-π* states, possibly accompanied by a minor contribution from metal-to-ligand charge transfer (MLCT) transitions. Compared with the phosphorescence induced by Ir(III) ion in the respective Ir(III) ppy-type complexes (Hppy = 2-phenylpyridine), **35** and **36** demonstrated extremely temperature-sensitive phosphorescent emissions with longer lifetimes. Moreover, the notable bathochromic behavior was observed in the emission peaks of **35** and **36** as compared to the corresponding metallated ligands, indicating their more extensive conjugation induced by *trans*-$Pt(PBu_3)_2$ units. **35**-based PLEDs showed a yellow electrophosphorescence with the best η_{ext} of 0.50%, η_L of 1.59 cd A^{-1}, and η_p of 0.60 lm W^{-1}. Devices fabricated from **36** exhibited an orange emission, and the optimum efficiencies were determined to be: η_{ext} = 0.67%, η_L =1.55 cd A^{-1}, and η_p = 0.55 lm W^{-1}. Apart from the phosphorescence induced by Ir(III) unit, the Pt(II) moiety can also facilitate SOC to produce their triplet emission. An energy transfer should occur from the Pt(II)-induced triplet states with high energy to the Ir(III)-induced low-energy triplet states, which results in the good color purity of emission and the enhanced phosphorescence intensity of the Ir(III) unit.

Copolymers **37a**-**37d** and **38a**-**38d** also demonstrated efficient triplet energy transfer from the Pt(II) skeleton to the Ir(III) segment that contributed to their intensive phosphorescence.[36] The high triplet energy level can suppress the undesired reverse energy transfer to improve the phosphorescence abilities in these copolymers (Figure 7e). **37a**-**37d** and **38a**-**38d** exhibited predominant yellow and red phosphorescence emissions at around 555 nm and 632 nm, respectively, while the phosphorescence intensities were enhanced with the increased proportion of the Ir(III) segment. The solution-processed PLEDs based on copolymers **37a**-**37d** revealed a yellow phosphorescence with the η_L of 11.49 cd A^{-1}, η_{ext} of 4.38%, and η_P of 3.78 lm W^{-1}, whilst the devices fabricated by **38a**-**38d** demonstrated remarkable performance with the η_L of 5.86 cd A^{-1}, η_{ext} of 10.1% and η_P of 2.29 lm W^{-1}. These studies demonstrate the broad application prospects of bimetallic conjugated polymers in the OLED field.

A series of phenyl-bridged bimetallic Au(I) complexes were reported by Chou and co-workers, in which the effective distance between the Au(I) ions and the emitting ππ* chromophores can be adjusted by changing the number of phenylene spacers.[37] This work illustrates that the elongation of effective distance can lead to the manipulation of both $S_1 \rightarrow T_1$ ISC rate and $T_1 \rightarrow S_0$ phosphorescence radiative decay rate constant, resulting in the decreased intensity ratio of the phosphorescence to fluorescence. Complex **39c** was selected as the dopant for the emissive layer (EML)

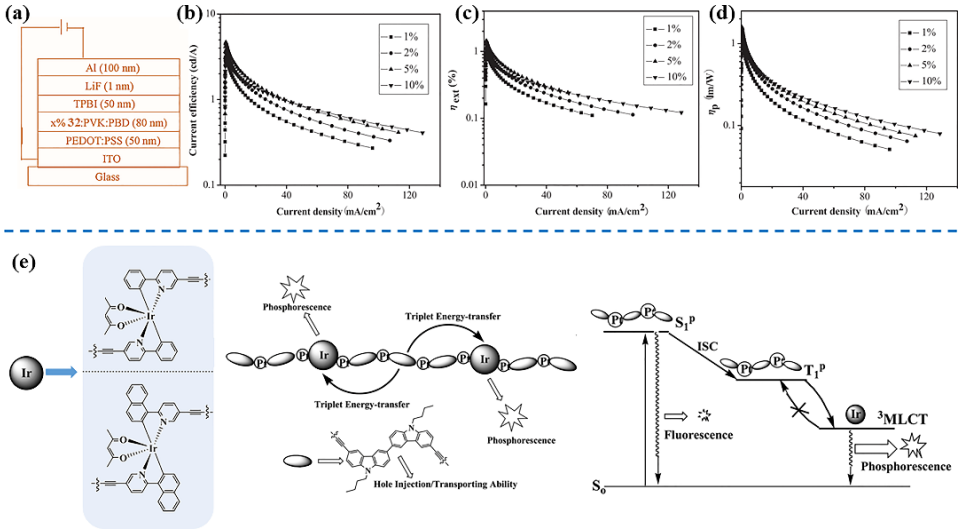

Figure 7 (a) The general configuration of PLED devices. (b) Current efficiency, (c) EQE, (d) power efficiency versus current density characteristics of polymer **32**-based PLEDs with different doping concentrations. Reproduced with permission from ref. 32. Copyright 2009, Wiley-VCH. (e) The schematic diagram of the structures and energy-transfer process in polymers **37a**-**37d** and **38a**-**38d**. Reproduced with permission from ref. 36. Copyright 2015, The Royal Society of Chemistry.

OLED to investigate the feasibility of generating white light based on fluorescence and phosphorescence dual emissions. The emissions of the as-prepared device covered the visible wavelengths from 380 to 750 nm, contributing to the white emission with high color-rendering index (CRI = 89.2-92.2).

3.1.2. OSCs

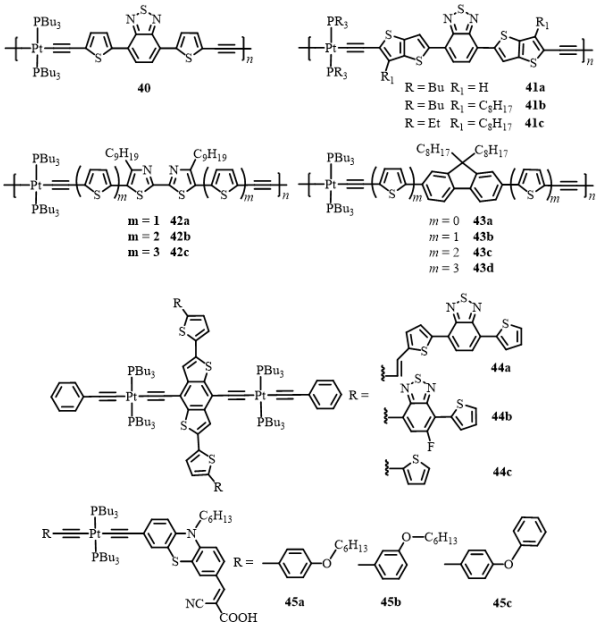

The development of photovoltaic materials brings an achievable tactic to alleviate the worldwide energy shortage, which involves the utilization of clean and sustainable solar energy for electricity generation.[38,39] Therefore, the efficient and economical solar cells are urgently needed for energy conversion, while the utilization of conjugated polymers with synthetic variabilities provides a flexible and tractable way to fabricate solution-processed polymer solar cells. Specially, Pt(II)-containing acetylenic polymers with tunable bandgaps, excellent electron transport capabilities and rich photophysical properties are outstanding candidates to be deployed as donor materials in bulk-heterojunction (BHJ) solar cells, thereby offering a cost-effective and light-weight energy conversion platform.[4, 40]

The narrow-bandgap metallopolyyne **40** bearing the 4,7-di-2'-thienyl-2,1,3-benzothiadiazole D-A structure was exploited, which exhibited extended absorption.[41] Such dark purple polymer showed a strong absorption peak at 554 nm and its narrow bandgap (1.85 eV) is much lower than those of polymer **2b** containing purely electron-rich bithienyl spacer (2.55 eV) and its counterpart with electron-deficient benzothiadiazole spacer (2.20 eV).[5] No triplet emission was observed in **40**, which is in line with the energy gap law of polyplatinaynes, indicating that the efficient photo-induced charge separation is mainly ascribed to the charge-transfer excited state rather than the triplet state.[16] The BHJ solar cells were successfully constructed by employing **40** and [6,6]-phenyl-C_{61}-butyric acid methyl ester (PCBM) as the electron donor and acceptor, respectively (Figure 8a-c). The effects of solvent, solution concentration and spinning speed were investigated to optimize the fabrication conditions of **40**/PCBM blend devices. The *J-V* curves under different illumination powers and the power dependences of the cell parameters are illustrated in Figure 8d-f. The as-prepared devices demonstrated high average power conversion efficiency (PCE) up to 4.1% with the open-circuit voltage (V_{oc}) of 0.82 V, the short-circuit current density (J_{sc}) of 13.1 mA cm^{-2}, and the fill factor (FF) of 0.37%. **40**-based PSCs displayed superior performance over that of the oligothiophene series, owing to the enhanced absorption in the visible-light region and the more balanced charge transport in polymer **40**. This work is a significant breakthrough for the development of PLEDs based on organometallic polymers. Amorphous Pt(II)-containing polyynes **41a**-**41c** bearing thieno[3,2-*b*]thiophene (TT)-2,1,3-benzothiodiazole linkers were reported by Jen and co-workers, which exhibited the absorption

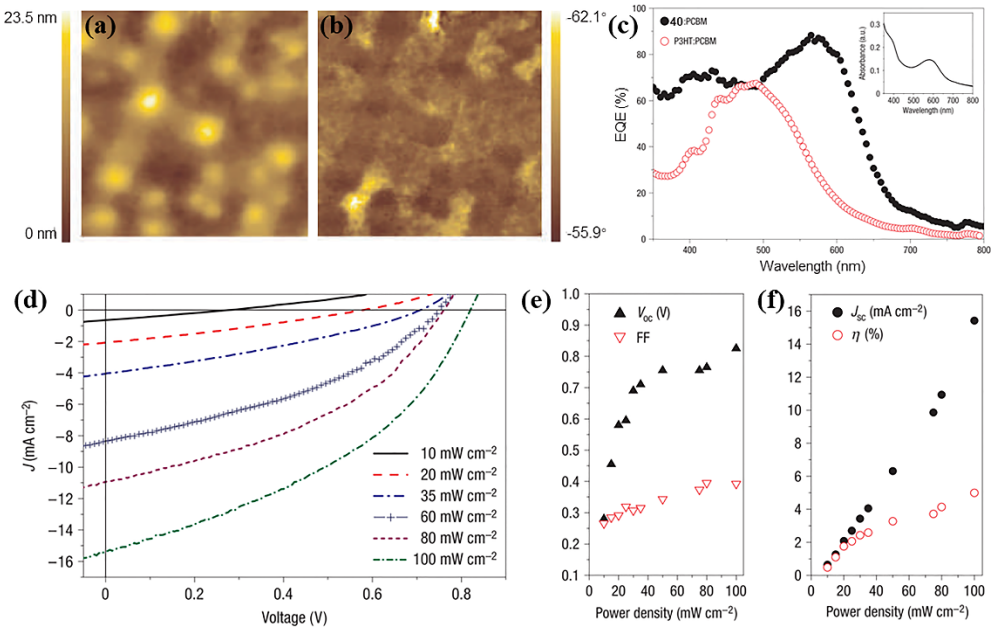

Figure 8 (a) Topography and (b) phase contrast images of **40**/PCBM (1:4) films. (c) The EQE and wavelength dependencies in **40**/PCBM (1:4) and poly(3-hexylthiophene) (P3HT)/PCBM (1:4) blend solar cells. The inset is the absorption of the **40**/PCBM active layer. (d) J-V curves under different illumination powers. Power dependences of (e) open-circuit voltage and fill factor, (f) short-circuit current density and power-conversion efficiency of the **40**/PCBM device. Repro-duced with permission from ref. 41. Copyright 2007, Springer Nature.

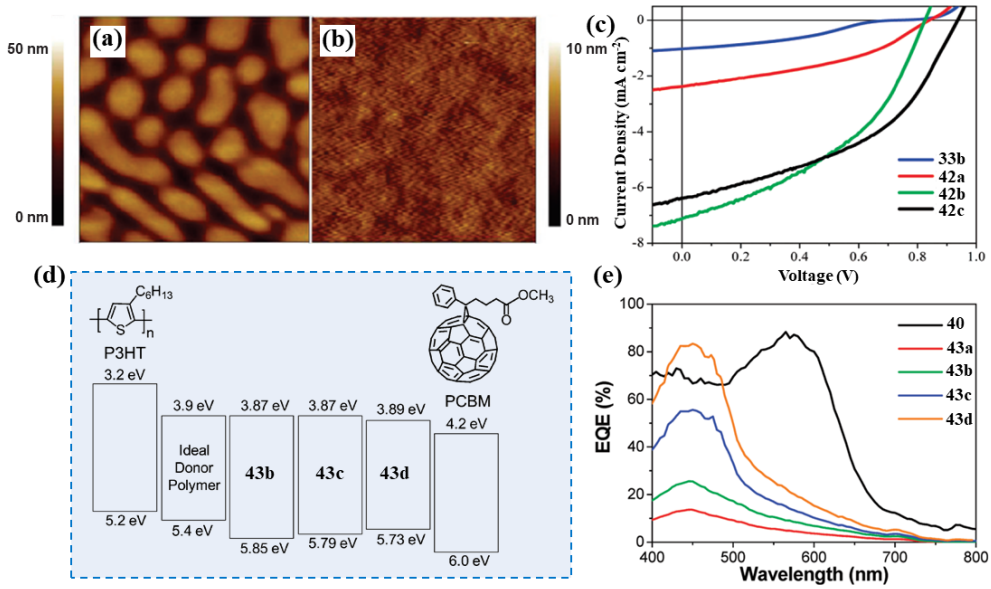

Figure 9 (a) AFM topography images of (a) **42b**/PCBM (1:4) and (b) **42b**/PCBM (1:5) blend films. (c) *J-V* curves of **33b**, **42a**-**42c**/PCBM (1:4) solar cells. (d) Band-structure diagram of **43b**-**43d**, P3HT, and an ideal donor relative to PCBM. Minus sign is omitted for the energy values. (e) EQE and wavelength dependencies in **40**/PCBM (1:4) and **43a**-**43d**/PCBM (1:5) blend solar cells. (a), (b), (d) and (e) were reproduced with permission from ref. 4. Copyright 2010, American Chemical Society. (c) was reproduced with permission from ref. 43. Copyright 2007, American Chemical Society.

spectra peaking at 587-611 nm in the solid state and low bandgaps in the range of 1.81-1.85 eV, owing to the intramolecular charge transfer (ICT) between the electron donors and acceptors.[42] The inclusion of more rigid TT units into **41a** leads to its enhanced hole mobility (μ_h) of 1.5×10^{-3} cm^2 V^{-1} s^{-1} compared to **40** (6.1×10^{-5} cm^2 V^{-1} s^{-1}). Moreover, μ_h can be further promoted to 1.0×10^{-2} cm^2 V^{-1} s^{-1} by incorporating alkyl chains into the TT segments of **41b** and **41c**, which is ascribed to the amorphous thin film characteristics caused by the steric hindrance between the bulky Pt(II) blocks. Thus, the introduction of spacers with more rigid structures is beneficial to the electron coupling between the electron donors and acceptors along the conjugated backbone, thereby enhancing the charge transport in these polyplatinaynes. Solar cell based on $PC_{71}BM$ and **41c** afforded the best performance with the PCE of 4.13%, V_{oc} of 0.79 V, J_{sc} of 10.12 mA cm^{-2}, and FF of 51.4%. Besides, different from the polycrystalline polymers, the thermal annealing will not lead to the improvement of cell performance in these Pt(II) polyyne systems due to their amorphous characteristics, which are less sensitive to the post-processing operation.

Polyplatinaynes **33b** and **42a**-**42c** with bis(oligothienyl)-2,2'-bithiazole D-A hybrid spacers realized the tuning of PSC efficiencies, optical properties and charge transport capabilities by regulating the number of oligothienyl rings in such organometallic systems.[43] The charge separation in the energy conversion process of **33b** and **42a**-**42c** is attributed to the charge-transfer excited state rather than the triplet state, since their low bandgaps induced by strong charge-transfer interaction is detrimental for the triplet emission while the increased heteroaryl rings in the ligands may impair the ISC induced by the Pt(II) center. A clear reduction of ca. 0.34 eV is found in the optical bandgap of **42c** (2.06 eV) compared with **33b** (2.40 eV) as the thienyl chain is extended. These solution-processable polymers showed intense absorption peaks in the spectra, rendering them suitable candidates for the construction of BHJ-type PSCs. The phase separation of **42b**/PCBM (1:4) blends can be observed from the atomic force microscopy (AFM) images, while the **42b**/PCBM (1:5) blend films exhibit smooth morphology (Figure 9a and b). The small-scale phase separation in **42b**/PCBM (1:4) films contributed to exciton dissociation and charge transport, leading to the reduced recombination losses and increased J_{sc}. As shown in Figure 9c, a distinct increase in the J_{sc} was detected in **42b** and **42c** as compared to **33b** and **42a**. Solar cells prepared by **42b** and PCBM demonstrated the PCE of 2.7% and the peak external quantum efficiency (EQE) of 83%, while both of the light-harvesting capabilities and PCEs of the prepared devices can be improved by increasing the thienyl chain length.

As for metallated polyynes **43a**-**43d** with bis(oligothienyl)-2,7-fluorene spacers, the E_g of orange-red **43d** with more thienyl rings is significantly reduced by ca. 0.60 eV than that of pale-yellow **43a** bearing purely fluorene spacer.[44] The cells based on **43a**-**43d** showed relatively high efficiencies owing to their high absorption coefficients (ε) and applicable energy levels for the interaction with PCBM (Figure 9d and e). However, it is not recommended to extend the conjugation length by introducing too many thiophene rings, which will increase synthetic complication and reduce the product yields. Solar cells based on **43d** revealed the optimal PCE of 2.9% and the peak EQE of 83%. Thus, these studies illustrated an attractive tactic to regulate the optical properties and photovoltaic performance of metallated conjugated polymers by increasing the number of thienyl rings for efficient power generation.

Research endeavors have also been focused on the development of small-molecule bulk heterojunction (SMBHJ) solar cells, which demonstrate well-defined structures and satisfactory photovoltaic performance.[40,45] "Roller-wheel"-shaped molecules **44a**-**44c** are synthesized by binding the Pt(II)-bisacetylide units with the short axis of a linear organic chromophore, which results in the partial overlap between the adjacent chromophores in a "slip-stack" manner, leading to the enhancement of both crystallinity and charge mobility.[46] The single crystals of **44a** unambiguously proved this slip-stack geometry in the solid state, whereas no π-π interaction between the chromophores was observed from the single crystal structure of **44c** . Although no single crystals were obtained from **44b**, it showed improved intermolecular interactions compared to **44c**. The E_g of **44a** and **44b** are 1.97 eV and 1.94 eV, respectively, which are much lower than that of **44c** (2.53 eV). Furthermore, the different physical and electronic

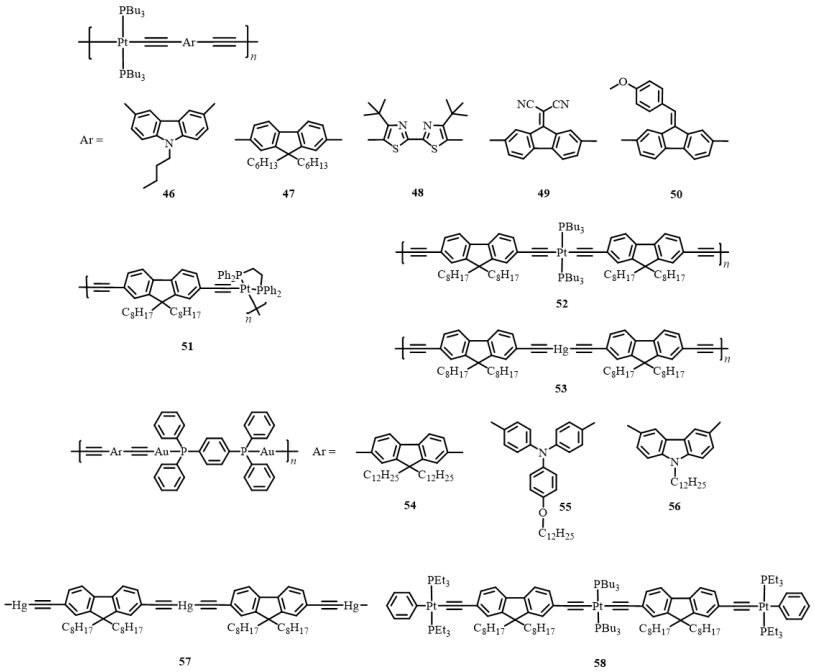

properties of **44b** and **44c** are ascribed to the variation in the length of linear chromophores (the rollers). From transient absorption measurements and theoretical calculations, the long-lived triplet states in these compounds exhibited both π-π* and ICT characters. Solar cells based on low-bandgap **44b** demonstrated an impressive PCE of 5.6% with the V_{oc} of 0.82 V, the J_{sc} of 11.9 mA cm^{-2}, and the FF of 57%. The material crystallinity is a key factor determining the performance of these devices. The lower bandgap and improved intermolecular interaction in **44b** are ascribed to its superior photovoltaic performance than that of **44c**. Compared with **44a**, **44b** with a shorter chromophore is less crystalline, which provides a wider window for structural modification, leading to the optimized morphologies after solvent vapor annealing operation and the high efficiency of **44b**.

As one of the promising categories of OSCs, dye-sensitized solar cells (DSSCs) have gained considerable attention owing to their low manufacturing cost, flexible and easy device construction, as well as satisfactory efficiency.[47] The structure and working mechanism of DSSCs have been depicted in many leading reviews.[48-52] A series of unsymmetrical phenothiazine-based photosensitizers **45a**-**45c** bearing different arylacetylide electron donors were prepared for high-efficiency DSSCs.[53] The utilization of π-bridging phenothiazine units with unique butterfly conformation can sufficiently prevent the molecules from aggregation, whilst cyanoacrylic acid is deployed as the electron acceptor and anchoring group. The distinct absorption bands of **45a**-**45c** located in the regions of 300-400 nm and 400-600 nm are originated from the π-π* transition and the ICT transition between the different donor-acceptor pairs, respectively. Besides, the bandgaps of these molecules are centered in the range of 2.22-2.27 eV. The DSSC fabricated with **45a** displayed the best PCE of 5.78% due to its high J_{sc} of 10.98 mA cm^{-1} and V_{oc} of 0.738 V, illustrating that the hexyloxyphenyl unit in the *para* position is a suitable donor in such systems. Cells based on **45b** and **45c** also gave good performance with the PCE of 4.43% and 4.34%, respectively. From the investigations, changing the position of the alkoxy chain will not influence the absorption, HOMOs/LUMOs and energy levels in these compounds to a large extent, but has a clear impact on the photovoltaic performance of DSSCs by governing the electron lifetime and charge-transfer resistance. This work provides a promising avenue for the establishment of DSSCs based on platinum-acetylide complexes.

3.1.3. OTE devices

The development of OTE materials offers a promising strategy to circumvent the global energy crisis, recycling the waste heat to generate electricity in an environmentally friendly way. Metallopolymers are potential materials for OTE devices, since the incorporation of metal centers leads to the enhanced electrical conductivity, whilst the organic backbones can be employed as suitable heat insulators.[54] The conversion efficiency of OTE materials can be evaluated by the dimensionless figure of merit $ZT = S^2\sigma T/\kappa$, where S is Seebeck coefficient (V K^{-1}), σ is electrical conductivity (S cm^{-1}), T is absolute temperature (K), and κ is thermal conductivity (W m^{-1} K^{-1}). Hence, the reasonable combination of conjugated polymers with high S and low κ, and the single-walled carbon nanotubes (SWCNTs) with high σ and mechanical robustness will definitely contribute to the production of high-performance TE composites.[55]

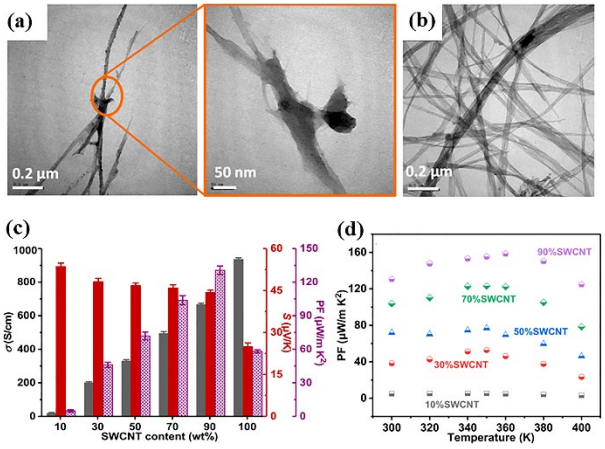

Figure 10 Transmission electron microscopy (TEM) images of **40**/SWCNT composites with the ratios of (a) 5:5 and (b) 1:9. (c) The histogram of σ, S and PF of polymer **40** versus different SWCNT loading. (d) PF and temperature dependencies in **40**/SWCNT composites with different SWCNT loading. Reproduced with permission from ref. 55. Copyright 2019, MDPI.

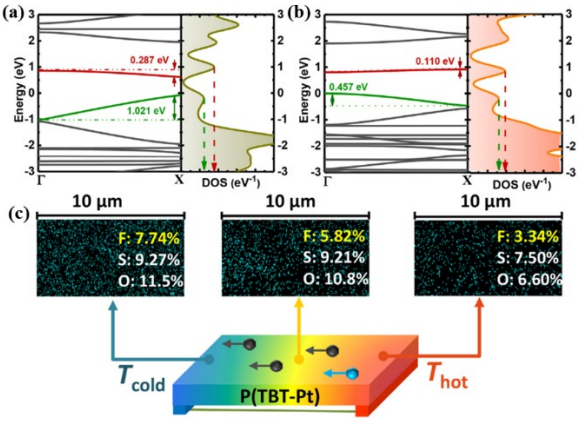

Figure 11 Band structure and partial DOS (the valence band is defined as 0) of (a) purely organic counterpart and (b) polymer **40**. (c) The EDS images of the F, S and O percentages of polymer **40** after treatment with TFSA under the temperature gradient of 10 °C. Reproduced with permission from ref. 56. Copyright 2021, Elsevier B.V.

In the Pt(II)-containing acetylide polymer **40**, the inclusion of planar Pt(II)-acetylide block into the π-conjugated architecture leads to a significant enhancement of the intermolecular interaction between **40** and the SWCNT, while the ligands in Pt(II)-acetylide unit can restrain the π-π stacking between the polymer backbones, thereby promoting the TE performance of the composites (Figure 10). As shown in Figure 10a, the polymers distributed evenly in the SWCNT frameworks, while the SWCNTs were wrapped well by the polymeric chains. With the increase of the SWCNT loading content (from 10% to 90%), the *S* of the hybrid films based on polymer **40** and SWCNT decreased slightly (from 53.5 ± 1.3 $\mu V \cdot K^{-1}$ to 44.3 ± 0.9 $\mu V \cdot K^{-1}$), whilst the σ and corresponding PF value of the composites gradually enhanced. Impressively, a PF value of 158.6 $\mu W \cdot m^{-1} K^{-1}$ was obtained from the temperature-dependent TE performance of **40**/SWCNT composites (Figure 10c and d). Importantly, the energy levels and bandgaps have a significant impact on the activation energy of charge carriers, determining the performance of OTE materials. The optimized power factor (PF) of the obtained composite is up to 130.7 $\mu W\ m^{-1} K^{-2}$ at ambient temperature, which is much higher than that of the composite containing the corresponding analogue without Pt(II) blocks (59.5 $\mu W\ m^{-1} K^{-2}$).

Generally, organic semiconductors in OTE applications can be classified as p-type (hole conduction) and n-type (electron conduction) depending on the paths of charge transport. However, the utilization of n-type materials in OTE field is hindered by the inefficient n-doping and electron trapping.[56] The insertion of heavy metal atoms into the conjugated backbones leads to the fabrication of satisfactory OTE devices by density of states (DOS) engineering, as the overlap between the sp_x orbitals of Pt(II) center and the σp_x orbitals of the conjugated ligand can increase their DOS nearby the Fermi level of the polymers. As compared with the respective organic polymer without Pt(II) center and acetylene segments, the improved DOS nearby the Fermi level of the polymer can be achieved in polyplatinayne **40** (Figure 11a and b). Furthermore, interfacial engineering of the polymer films was conducted to endow such system with dual electronic-ionic transport feature by the surface protonation utilizing trifluoromethanesulfonic acid (TFSA). Consequently, n-type self-doping behavior was determined in the as-prepared films owing to the anion-induced electron transfer between the $CF_3SO_3^-$ anions and the ionized π-acidic backbones, thereby promoting the electronic conductivity of the polymer **40**-based films. As shown in Figure 11c, the $CF_3SO_3^-$ migration can be observed by energy dispersive spectroscopy (EDS) measurements of polymer **40** under the studied temperature gradient of 10 °C, which accounts for its high thermopower (α). The OTE devices based on polymer **40** demonstrated superhigh α over -3150 $\mu V\ K^{-1}$ with a favorable σ of 17.1 $S\ m^{-1}$, giving one of the best results of n-type OTE materials. This work provides a strong evidence for the vast prospect of metallopolyynes in the OTE field.

3.2. Nonlinear optics

The construction and performance optimization of NLO materials have greatly promoted the development of related applications, including OPL, data processing, optical switching and optical communication, etc. Metallated polyynes are attractive NLO materials, since the incorporation of polarizable low oxidation state metals with occupied *d*-orbitals into the conjugated backbone results in the extended conjugation length to increase the hyperpolarizability. Notably, as the rapid development of laser technology, high-performance OPL devices are urgently needed to deal with the damage of laser pulses to human eyes and sensitive optical elements. The representative OPL mechanisms have been expatiated in our previous review,[57] among which reverse saturable absorption (RSA) and two-photon absorption (TPA) are two prevalent paradigms for the construction of OPL devices, whilst the Z-scan method is the most commonly utilized technology to evaluate the RSA and TPA behaviors in the OPL materials.

A series of high-performance optical power limiters have been fabricated successfully through the design and synthesis of molecular/polymeric metallaynes. In 2005, the OPL capabilities of polyplatinaynes **2b** and **46**-**50** were studied for the first time (Figure 12a).[58] The OPL capabilities of polymers **46** and **47** are mainly derived from the triplet absorption, whereas the ICT contributes to the OPL responses in polymers **2b** and **48**-**50** due to the D-A structure in their main chains. All these polymers exhibited low optical limiting thresholds (F_{th}) in the range of 0.06 to 0.15 J cm^{-2} at the linear transmittance (T_o) of 82%. **46**, **48** and **49** demonstrated comparable OPL performance to C_{60} solution, while the OPL ability of **2b**, **47**, and **50** is even superior to that of C_{60}.

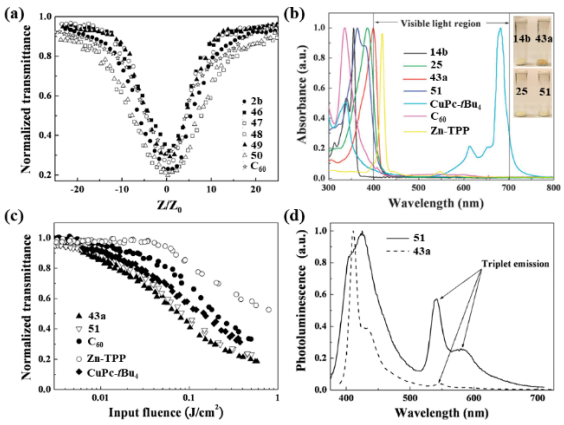

Figure 12 (a) Z-scan curves of polyplatinaynes **2b**, **46**-**50** containing different aromatic ligands and that of C_{60} solution (T_o = 82%). (b) Optical transparency of fluorene-based polymetallaynes **14b**, **25**, **43a**, **51** and that of three conventional OPL materials (CuPc-*t*Bu_4, C_{60} and Zn-TPP). The inset is the photograph illustrating the light colors of these polymetallaynes. (c) OPL performance of **43a**, **51** and the benchmark dyes. (d) PL spectra of **43a** and **51** in CH_2Cl_2 at room temperature. Reproduced with permission from ref. 57. Copyright 2011, The Royal Society of Chemistry.

Table 1 The OPL performance of impressive polymetallaynes and molecular metallaynes.

Compound	F_{th} [a] (J cm^{-2})	T_o [b] (%)	L [c] (mm)	σ_{ex}/σ_o [d]	Reference
14b	0.11	92	1	20.81	[31]
25	0.08	92	1	18.32	[31]
43a	0.07	92	1	19.07	[31]
51	0.08	92	1	18.62	[31]
57	0.13	92	1	17.27	[31]
58	0.07	92	1	17.91	[31]
59	0.1	92	1	13.0	[61]
60	0.05	92	1	14.0	[61]

[a] Optical-limiting threshold. [b] Linear transmittance. [c] Sample thickness. [d] σ_{ex} and σ_o are the effective excited-state and ground-state absorption cross sections, respectively.

Apart from the outstanding OPL efficiency, **47** also displayed satisfactory transparency (λ_{max} < 400 nm), indicating its optimized OPL/transparency trade-off. However, the relatively poor transparency of **2b** and **48**-**50** with electron-withdrawing and electron-donating moieties suggests that the introduction of D-A structure to the polymer backbone is not conducive to the comprehensive optimization of transparency and OPL activation. Besides, nearly all the polymeric metallaynes exhibited superior OPL performance to that of their corresponding dimers owing to the π-electron conjugation along the polymer backbone through the interaction between the *d* orbitals of Pt(II) centers and the π orbitals of the ligands. Therefore, the authors put forward two effective approaches to improve OPL performance in metallated polyynes: one is by employing heavy metal atom to improve the triplet state yield through the enhancement of ISC rate, another one is by fabricating suitable D-π-A architectures in the conjugation path to facilitate the generation of ICT states.

Inspired by the excellent OPL/transparency trade-off in **47**, a series of polymetallaynes with single or dual metal centers have been prepared to investigate the influence of different metal centers on the OPL performance.[31] For **43a**, **14b** and their Pd(II)-containing congener, the nature of metal ions plays a crucial role in determining their OPL responses. Compared with **14b** and its Pd(II)-containing congener, **43a** demonstrated better OPL performance owing to its higher triplet state quantum yield (Φ_T) at ambient temperature. Moreover, the OPL effect of **14b** is much better than that of Pd(II)-polyyne due to its strong absorption of ICT states. Consequently, the promoting effect of different metal centers with same ligands on the OPL performance in such metallated polyynes follows the order: Pt(II) > Hg(II) >> Pd(II). As shown in Figure 12b, **43a** (λ_{max} = 399 nm and $\lambda_{cut\text{-}off}$ = 417 nm) and **14b** (λ_{max} = 355 nm and $\lambda_{cut\text{-}off}$ = 370 nm) are both white solids with superior visible-light transparency to that of Pd(II)-containing polyyne (λ_{max} = 412 nm and $\lambda_{cut\text{-}off}$ = 442 nm), making the former two polymers excellent candidates as optical limiters.

Sequentially, heteronuclear alkynyl polymers **25**-**27** were studied for the trade-off issue between OPL and transparency. Heterometallic polyynes **25** and **26** gave higher Φ_T and lower fluorescence quantum yield (Φ_F) as the presence of Pt(II) blocks induced strong SOC effect, contributing to their enhanced OPL ability in comparison with the corresponding Hg(II) or Pd(II)-based mononuclear polyynes. On the contrary, the incorporation of Pd(II) units in **26** and **27** leads to their weaker OPL responses than those of **43a** and **14b** with only Pt(II) or Hg(II) centers. It is worth noting that the inclusion of Hg(II) ions into **25** and **27** endows them with better OPL effect than that of the respective mononuclear Pt(II)- and Pd(II)-containing polyynes, which is attributed to the conjugation interruption effect of Hg(II) ions.

The similar conjugation interruption strategy is also applied to **51** by switching the geometry of Pt(II)-block from *trans*- to *cis*-structure to realize the balance of OPL capability and optical transparency.[59] White polymer **51** also exhibited an impressive transparency with the λ_{max} and $\lambda_{cut\text{-}off}$ of 364 nm and 406 nm, respectively, in which the λ_{max} value afforded a distinctly blue-shift, confirming the effective conjugation interruption induced by such a *cis*-structure (Figure 12b). From Figure 12c, **51** showed comparable OPL effect to **43a**, demonstrating that the loss in OPL caused by conjugation interruption can be compensated by the positive contribution of the significantly enhanced Φ_T in such systems. This result can also be proved by the much stronger triplet emission of **51** than that of **43a** at 298 K (Figure 12d). Besides, the effects of metal ion content and conjugation length on the OPL capability were also studied in detail. **52** and **53** with less metal ion contents in their backbones gave weaker OPL responses compared to **43a** and **14b**, since the increased conjugation length in their ligands can reduce the contribution of metal centers and generate more π→π* transition localized on the ligands, leading to the decreased SOC and Φ_T. Besides, the organometallic trimers **57** and **58** displayed

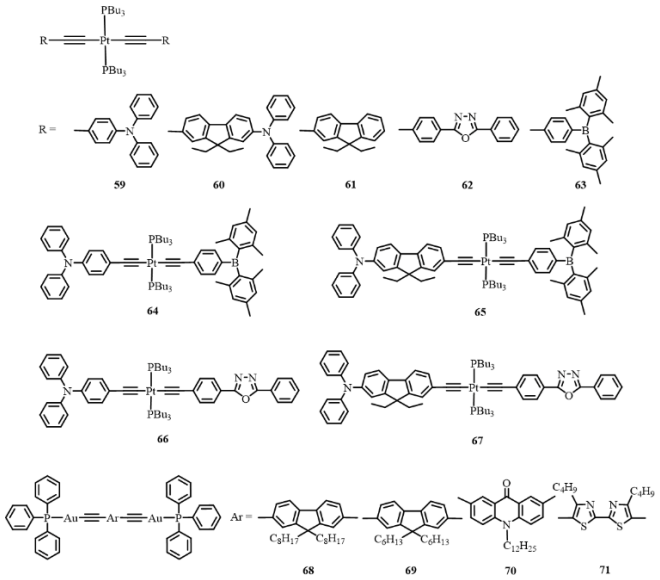

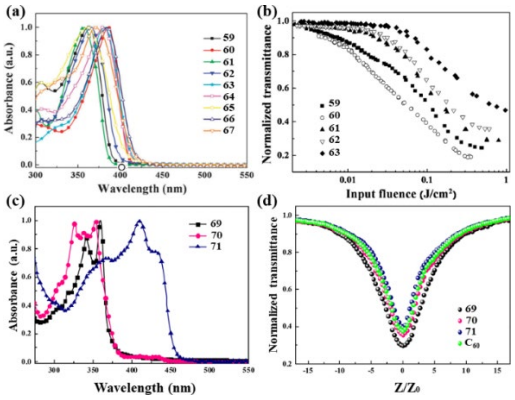

Figure 13 (a) UV-vis absorption spectra of the symmetric and asymmetric Pt(II)-containing acetylides **59**-**67** in CH_2Cl_2 at 293 K. (b) Normalized transmittance versus incident fluence of the symmetric Pt(II)-containing acetylides **59**-**63** in CH_2Cl_2 (T_o = 92%). Reproduced with permission from ref. 57. Copyright 2011, The Royal Society of Chemistry. (c) UV-vis absorption spectra of the Au(I)-containing acetylides **69**-**71** in CH_2Cl_2 at 298 K. (d) Open-aperture Z-scan results of Au(I)-containing acetylides **69**-**71** (T_o = 90%) and C_{60} (T_o = 85%). Reproduced with permission from ref. 62. Copyright 2016, Elsevier B.V.

almost the same OPL responses compared with the corresponding polymers **14b**, **43a** and **25**, indicating that the further extension of conjugation length beyond two repeating units would not lead to the significantly positive effect on OPL properties of these metallaynes.

The enhanced triplet emission was also observed in soluble Au(I)-containing polyynes **54**-**56**.[60] The absorption of **54**-**56** located in UV region endowed them with outstanding visible-light transparency, whilst their OPL effect was proved to rely on the RSA mechanism of the triplet excited states. **54** and **55** both demonstrated superior OPL ability than that of C_{60}, and a prototype OPL device was fabricated by doping **54** to the polystyrene solid matrix. The as-prepared device realized a further promotion of the OPL performance compared to that in the solution state, hence providing an important method for the development of novel OPL devices.

The impact of molecular symmetry and the electronic properties of ligands on the OPL performance were investigated in symmetric and unsymmetric Pt(II)-containing bis(acetylide) complexes **59**-**67**.[61] These compounds all exhibited excellent optical transparency in the visible-light window, while the variation in the triplet state character of **59**-**67** resulted in their different OPL properties (Figure 12a and b). From the time-dependent density functional theory (TD-DFT) calculations, the excited state character in **59** and **60** with two electron-donating groups (D-Pt-D type) is dominated by the ligand-to-metal charge transfer (LMCT) states, whilst **62** and **63** bearing electron-accepting moieties (A-Pt-A type)mainly exhibit triplet states with considerable MLCT character. As for unsymmetric complexes **64**-**67** (D-Pt-A type), their excited states mostly consist of the ligand-to-ligand charge transfer (LLCT) character. Consequently, the OPL performances in these Pt(II)-bis(aryleneethynylene)s follow the order: D-Pt(II)-D > D-Pt(II)-A > A-Pt(II)-A. Except for **63** and **66**, complexes **59**-**67** all showed stronger OPL capability than that of C_{60}. **59**-**67** manifested sizable σ_{ex}/σ_o values in the range of 9-17, among which the F_{th} of **60** was as low as ca. 0.05 J cm^{-2} (T_o = 92%).

Among the Au(I) acetylides **68**-**71**, **68** demonstrated a remarkable transparency (λ_{max} = 361 nm and $\lambda_{cut\text{-}off}$ = 372 nm) and comparable OPL performance to C_{60} with the σ_{ex}/σ_o value of 9.76.[31,62] The electronic properties of ligands also play an important role in determining the OPL capability of these Au(I) complexes. As illustrated in Figure **13c**, **69** and **70** gave negligible absorption peaks in the visible-light region, leading to their better transparency compared with **71**. OPL effect in **69** and **70** was assigned to the RSA from the T_1 states due to the Au(I)-induced SOC effect, while the OPL behavior in **71** was governed by TPA mechanism. Although the electron-rich character of the organic spacers follows the order: bithiazole >> acridone > fluorene, the order of OPL capabilities in these complexes is: **69** > **70** > **71**, illustrating that the adoption of organic spacers with neither electron-rich nor electron-deficient property can improve the OPL effect in such Au(I)-acetylide systems (Figure 13d). At the T_o of 90%, **69** and **70** demonstrated even better and nearly identical OPL responses as compared with C_{60}, respectively, indicating that Au(I) acetylides possess tremendous applicable value for laser protection.

The extensively delocalized π-conjugated structure in 2D carbon materials allows them to become suitable frameworks for the construction of novel and adjustable NLO materials. Recently, free-standing mercurated graphyne organometallic nanosheets (MGONs) **21** and **22** were fabricated through the interface-assisted bottom-up method.[8] These MGONs were prepared at the interface between the aqueous solution of $HgCl_2$ and the hexane solution of the corresponding triacetylenic ligands. The polymerization of Hg(II) ions and the alkynyl monomers through *d*π-*p*π interactions enables the π-electrons to be delocalized along the whole conjugated frameworks, leading to the extension of π-conjugation. The bandgaps of **21** and **22** are variable in the range of 2.14 to 3.37 eV, while the DOS and the absorption characteristics are both dominated by the contribution of local *p*-orbitals. The NLO responses in these nanosheets were examined by open-aperture Z-scan technology with nanosecond laser at 532 and 1064 nm (Figure 5). **21** demonstrated higher modulation depths (A_s), SA intensities (I_s) and the corresponding nonlinear extinction coefficient values than those of **22** at the same input energy (E_0) under the laser irradiation of both 532 nm and 1064 nm, illustrating that **21** possesses the superior SA performance compared with **22**. The outstanding SA properties of **21** and **22** are ascribed to Pauli-blocking (band-filling effect) induced by Hg(II)-polyyne frameworks with periodic structures, leading to their great potentials in the fabrication of passive Q-switchers.

The PQS properties at 1064 nm were achieved successfully by using **21** and **22** as the saturable absorbers (Figure 14). Through the optimization of these nanosheets, the PQS performance of **21**- based nanosheets is comparable to conventional 2D materials (for instance, black phosphorus, graphene and

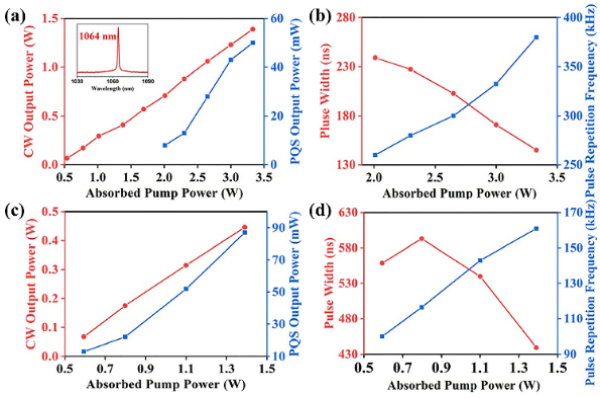

Figure 14 Passively Q-switched Nd:YAG laser properties with nanosheets **21** and **22** as the saturable absorbers. (a) Output power (the inset is the laser emission spectrum) and (b) pulse width and repetition frequency with **21** as the saturable absorber. (c) Output power and (d) pulse width and repetition frequency with **22** as the saturable absorber. Reproduced with permission from ref. 8. Copyright 2021, Wiley-VCH.

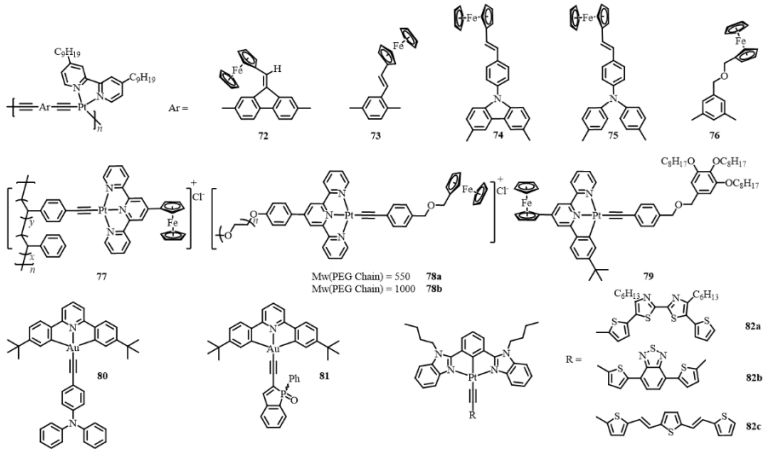

and MoS_2), whilst better pulse properties are observed in **22**. Importantly, the laser damage thresholds of nanosheets **21** and **22** at 1064 nm are 657 and 329 MW cm^{-2}, respectively, while the highest intracavity power densities of these nanosheets in the PQS laser experiments are determined to be 21.2 and 28.6 kW cm^{-2}, respectively. There was no thermal damage in these nanosheets during the PQS experiments and the output was very stable under the laser operation at high pump power, indicating the extremely high stability of the MGONs under intense laser irradiation. This report demonstrates the remarkable optoelectronic properties of the 2D organometallic nanosheets, which can lead to their good prospects for practical applications.

3.3. Data storage and memory devices

The fabrication of data storage and memory devices is of great significance to meet the demands of the rapidly developing computing technology. Generally, the storage and memory devices have different design specifications, data access standards and protocols.[63] The emerging memory technologies provide irreplaceable strategies to tackle the technical obstacles in conventional memory devices, where metallated organic compounds have demonstrated remarkable application potentials for their tunable photoelectric characteristics, rich structure-property relationships, film-forming abilities and solution processabilities.[64] Notably, magnetic random access memory (MRAM) and resistance random access memory (RRAM) can achieve the storage of information through novel physical mechanisms instead of relying on charge storage in the capacitor, making them promising options for the production of advanced non-volatile memory devices. In this section, the representative studies of MRAM and RRAM based on polymeric and molecular metallaynes will be respectively discussed.

3.3.1. MRAM

As an appealing non-volatile memory technology, MRAM with high density and high speed access time can regulate the magnetic properties of active materials for the storage of ''1'' and ''0'' binary information. There are different types of MRAM devices fabricated by organic compounds, including spin valves (SVs), magnetic tunnel junctions (MTJs), bit patterned media (BPM), etc. BPM can store one single bit of information in an individual nanostructure with the easy axis of magnetization out-of-plane.[65] It is worth noting that ferromagnetic alloy NPs (for example, $L1_0$-FePt NPs) are important storage media in BPM, which can be obtained by using metallated polymers or molecules as precursors.[66,67] A series of Fe(II)- and Pt(II)-containing bimetallic acetylide compounds have been developed for the preparation of $L1_0$-FePt NPs.

In 2008, polyferroplatinyne **72** with excellent stability in air and moisture was created successfully as the precursor for ferromagnetic FePt NPs, which is the first example of diimine stabilized *cis*-platinum polyyne.[68] The generation of undesired Fe_2P and PtP_2 phases after pyrolysis process can be avoided by replacing the phosphine ligands in Pt(II)-blocks by bipyridine-type ligands. The obtained FePt NPs show an average size of 4 nm with a narrow size distribution, while the well-faceted octahedral shape of these NPs indicates that they are highly crystalline (Figure 15a and b). From the energy-dispersive X-ray (EDX) elemental analysis, the ratio of Fe to Pt species is approximately 0.45:0.55 in the NPs, and the slight deviation from the 1:1 stoichiometric ratio is derived from the faster loss of potentially volatile Fe(II)-containing fragmentation products in comparison with the Pt(II)-containing ones during the pyrolysis process. As shown in Figure 15c and d, polymer **72** can be used directly as a negative resist to fabricate FePt NP patterns with high magnetocrystalline anisotropy through both electron-beam lithography and UV photolithography methods, endowing the patterns with excellent shape retention and well-defined edges.

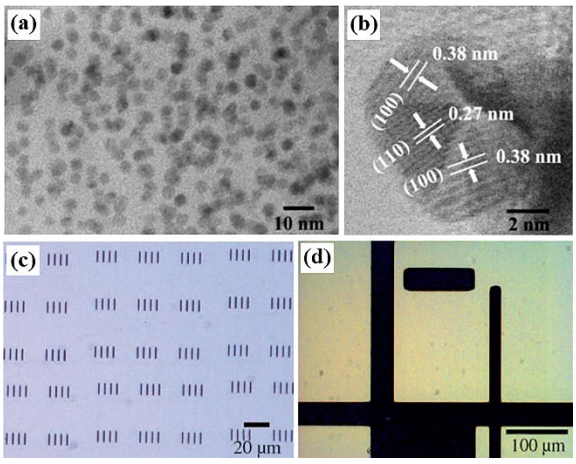

Figure 15 (a) TEM bright-field image of the nanoparticles prepared from polymer **72**, (b) high-resolution TEM (HRTEM) image of a single nanoparticle with octahedral shape. Optical micrographs of polymer **72** (c) microbars obtained by electron-beam lithography and (d) patterns fabricated using UV photolithography with a chrome contact mask. Reproduced with permission from ref. 68. Copyright 2008, Wiley-VCH.

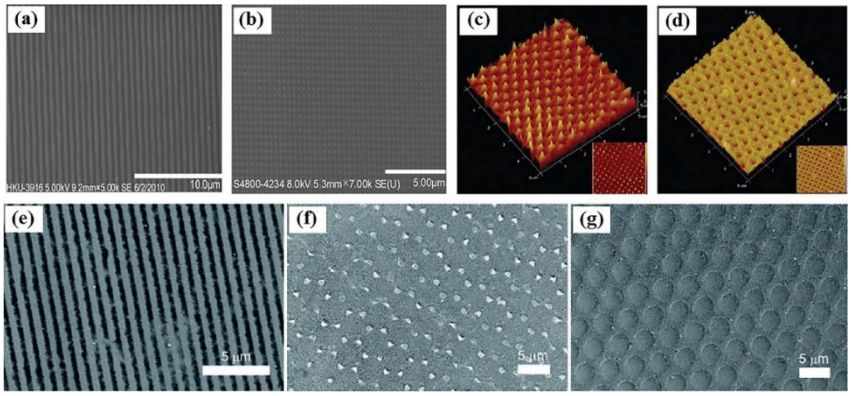

Figure 16 SEM images of the nanoimprinted (a) line array pattern and (b) dot array pattern of polymer **73**. MFM images of the nanoimprinted dot array pattern of FePt NPs field-annealed in the (c) -Z magnetic direction and (d) +Z magnetic direction. Reproduced with permission from ref. 66. Copyright 2012, Wiley-VCH. SEM images of the nanoimprinted (e) line array pattern, (f) hexagonal pillar array pattern and (g) hole array pattern of complex **79** after pyrolysis. Reproduced with permission from ref. 74. Copyright 2018, Springer Nature.

Generally, there are two solution-processed strategies to achieve BPM based on $L1_0$-FePt NPs: self-assembly and nanoimprint lithography (NIL). **73** with excellent solubility and film-forming ability was successfully used to prepare array patterns of $L1_0$-FePt NPs through the NIL technique (Figure 16a and b).[66] The $L1_0$-FePt NPs can be obtained directly after the pyrolysis of **73** without any post-annealing treatment, exhibiting spherical morphology and high crystallinity. The average size of the as-prepared NPs is confirmed to be 4.6 ± 1.2 nm with a narrow standard deviation, and the atomic ratio of Fe(II) to Pt(II) is approximately 1:1, which is in line with the stoichiometry in **73**. The nanopatterned samples showed a coercivity as large as 14 kOe at room temperature, and the prototype BPM based on **73** gave an areal density of 2.58 Gb in^{-2}. From the magnetic force microscopy (MFM) images, the magnetization direction of the patterned $L1_0$-FePt NPs can be manipulated to point ''up'' or ''down'' by applying an external magnetic field with alternate magnetic field directions (Figure 16c and d), thereby providing a promising platform for the development of magnetic recording systems.

Sequentially, FePt-containing metallopolymers **74** and **75** were prepared to further investigate the effect of pyrolysis temperature on the size and magnetic properties of the resulting FePt NPs.[69] It should be noted that these polyferroplatinynes possess low solubility in common organic solvents Nearly equiatomic $L1_0$-FePt NPs were obtained in a single step by employing **74** and **75** as the molecular precursors. Compared to the NPs synthesized from **74** with the average sizes in the range of 11.3-14.7 nm, NPs generated from **75** showed smaller particle sizes of 6.3-7.78 nm, which was ascribed to the higher onset decomposition temperature of **75**. Importantly, the average size of the prepared FePt NPs decreases with increasing the pyrolysis temperature, since the higher temperature leads to more rapid fracture of chemical bonds while the organic fragments can protect the FePt seeds from further sintering.[70] The resulting FePt NPs are in well-faceted spherical shape, whilst the NPs prepared from **75** demonstrate a higher coercivity than that of **74**-based NPs owing to their smaller particle size. Thus, for these two FePt-containing polyynes, a higher pyrolysis temperature endows the resulting $L1_0$-FePt NPs with both smaller size and larger coercivity.

76 with enhanced overall solubility in common organic solvents was fabricated by attaching the ferrocene to the aromatic ring spacer via a freely-rotating O-bridge. This structure endows **76** with improved solubility and solution processability, contributing to the construction of nanoscale patterns via NIL.[71] With the utilization of **76** as the single-source precursor, highly-ordered FePt NPs were successfully prepared after thermal annealing process under an Ar/H_2 (v/v = 95/5) atmosphere. These NPs exhibited regular shape with an average size of 12.7 nm and an ultrahigh coercivity of 36 kOe, as the presence of H_2 can facilitate the formation of face-centered tetragonal (fct) phase, whereas the NPs prepared in pure Ar existed as a mixture of the face-centered cubic (fcc) and fct phases. Nanoscale line and dot arrays for BPM were patterned successfully, demonstrating the application potentials of this method for ultra-high-density magnetic data storage.

The functional bimetallic unit is attached to the side chain of copolymer **77** for the synthesis of $L1_0$-FePt NPs, which exhibit a nearly equal atomic ratio for Fe to Pt species and spherical shape with an average size of around 7.4 nm.[72] Besides, polymer **77** showed good air-stability and thermal stability. However, the NPs synthesized from the corresponding molecular analogue of **77** belong to the $FePt_3$ phase with the atomic ratio of 30:70 (Fe:Pt). NPs prepared from **77** also displayed a higher coercivity of 7.2 kOe as compared with the NPs based on the small molecule (0.6 kOe), since the magnetic coercivity of FePt phase is higher than that of $FePt_3$ phase. These results indicate that the spatial structure of precursor possesses an important impact on the nucleation process of FePt NPs. Polymer **77** was successfully patterned by high-throughput NIL method, and the featured nanoline structures from the stamped template can be maintained after the pyrolysis of the patterned substrate. The organic skeleton was decomposed while the $L1_0$-phase FePt NPs were obtained in situ, indicating the feasibility of this strategy for the application of BPM recording media.

Amphiphilic metallopolymers **78a** and **78b** can be synthesized by attaching the hydrophilic poly(ethylene glycol) (PEG) chains to the hydrophobic bimetallic complex cores, in which the molecular weights of PEG chains are 550 and 1000, respectively.[73] The PEG tails can be utilized as the protective layer during pyrolysis while enable the NPs to disperse more evenly, suggesting that the particle size can be regulated by changing the length of the PEG chains to some extent. The average sizes of FePt NPs synthesized from **78a** and **78b** are measured to be 24.7 nm and 8.2 nm with the coercivities of 9.6 kOe and 1.3 kOe, respectively, and the higher coercivity of the former NPs is ascribed to their higher crystallinity. The discrepancy in the saturated magnetic moments of NPs based on **78a** (12.5 emu g^{-1}) and **78b** (6.1 emu g^{-1}) is derived from the different mass of PEG chains in these bimetallic precursors. Besides, the amphiphilic structure in such polymers enables the FePt-containing blocks to assemble together for the formation of PEG-tailed bimetallic aggregates, contributing to the uniform morphology of the resulting FePt NPs

Small molecular bimetallic complex **79** with hemiphasmidic structure was created as the single-source precursor for $L1_0$-FePt NPs.[74] The rigid coplanar bimetallic cores and the surrounding flexible tails in **79** lead to the spontaneous molecular arrangements, generating the highly ordered negative morphology replicated from the soft template. The inclusion of a dendritic group into **79** can achieve the effective regulation of the spatial property while weaken the molecular interactions, thus resulting in the relatively small average size of FePt NPs (9.5 nm). Besides, the as-prepared NPs showed nearly equal atomic ratio of Fe to Pt species, which also demonstrated the saturated magnetic moment of 25.3 emu g^{-1} in the magnetic field of 6.5 T with the coercivity of 10.6 kOe at room temperature. Importantly, the molecular structure of the precursor is a crucial factor in determining the size of NPs, but with negligible influence on their coercivities. Complex **79** was patterned successfully in line, hexagonal pillar and hole morphologies through NIL, indicating the practical utility of this strategy (Figure 16e-g). The line arrays prepared by using DVD-type soft template are suitable candidates for common DVD recording media. This work describes the approach to prepare ordered patterns by utilizing small molecular organometallic complexes as precursor for the first time, leading to their promising applications in magnetic data recording field.

3.3.2. RRAM

RRAM devices with simple components have aroused extensive research interest owing to their unique advantages, including good scalability, fast writing and reading, low power consumption, high switching endurance and large capacity for data storage. There are two electrical switching characteristics in RRAM devices: volatile and non-volatile types. Non-volatile switching can be classified into three categories according to the current-voltage curves: write-once-read many times (WORM) resistive switching, reversible unipolar switching, and bipolar switching behaviors. The exploration of organometallic materials for RRAM application has bright prospects, since the tunable structures and reversible redox processes in these compounds play an important role in the generation of electrical bistates and multistates.[63]

A series of Au(III)-acetylide complexes were reported by Yam's group for RRAM applications. Bis-cyclometalated compound **80** with donor-acceptor structure is the first example of small-molecule organometallic complex applied in organic memory.[75] The lower-energy band (391-408 nm) in the electronic absorption spectra of **80** is mainly ascribed to a metal-perturbed intraligand (IL) π-π* transition of 2,6-bis(4-*tert*-butylphenyl)pyridine (^{t}BuC^N^C^{t}Bu), while the structureless emission at around 600 nm is derived from the excited state with ^{3}LLCT character [π(C≡C−$C_6H_4N(C_6H_5)_2$-*p*)→π*(^{t}BuC^N^C^{t}Bu)]. The memory mechanism of **80**-based devices is assigned to the stable charge-separated state generated by the electron transfer from the electron donor (the diphenylamino substituent in phenylalkynyl moiety) to acceptor (^{t}BuC^N^C^{t}Bu unit) in an electric field. Consequently, the ITO/**80**/Al device demonstrated an impressive memory performance with the low operating voltage (2.2-2.8 V), the high ON/OFF current ratio (>10^5), the long retention time (>10^4 s), as well as the good stability.

Sequentially, phosphole oxide-containing Au(III) complex **81** was prepared by replacing the triphenylamine unit with benzophosphole oxide group.[76] As illustrated in Figure 17a, the spin-coated layer of **81** was utilized to fabricate the memory device (ITO/**81**/Al), which showed a smooth surface owing to the ordered molecular arrangement and weak π-π stacking in the complex thin film, contributing to the efficient charge transfer and the low threshold voltage (V_{th1} = 1.54 V, V_{th2} = 2.64 V). The ternary memory behavior in this device was confirmed by the two transitions in conductivity which represents two "writing" processes and the three conductive states (OFF, ON1, ON2) with different

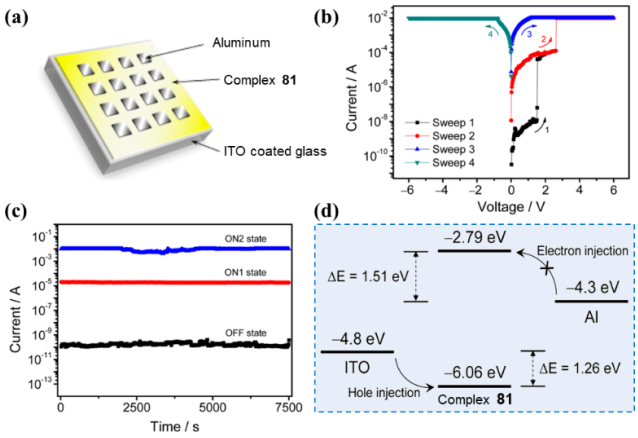

Figure 17 (a) The composition of the memory device fabricated by complex **81**. (b) Current-voltage characteristics of the device. (c) Stability of the memory device at different states under a constant voltage stress at 1 V. (d) Schematic diagram of the charge injection processes in the memory device. Reproduced with permission from ref. 76. Copyright 2016, American Chemical Society.

and the three conductive states (OFF, ON1, ON2) with different current ratios (1:10^3:10^7) (Figure 17b and c). Besides, the ON2 state can transfer to OFF state when the power is switched off, indicating the static random-access memory (SRAM) character of the as-prepared device. The HOMO and LUMO energy levels are measured to be -6.06 and -2.79 eV, respectively, and the energy gap is 3.27 eV (Figure 17d). The multilevel memory behavior in this device is ascribed to the two distinct charge-trapping sites in the tridentate ligand (^{t}BuC^N^C^{t}Bu) and the benzophosphole oxide unit, which demonstrates different electron-withdrawing abilities to stepwisely hinder the mobility of charge carriers. This work illustrates that the introduction of electron-accepting moiety to such cyclometalated alkynyl-Au(III) complexes can realize the manipulation of memory behavior and performance, thereby promoting the data storage capacities in organic memory systems.

Cyclometalated N^C^N Pt(II) alkynyl complexes **82a**-**82c** were prepared and applied in the construction of organic memory devices.[77] From the electrochemical examination, **82c** exhibited a less positive potential (+0.53 V vs SCE) than those of **82a** (+0.71 V vs SCE) and **82b** (+0.67 V vs SCE) due to the presence of more π-conjugated and π-donating oligothienylenevinylene alkynyl ligand, indicating that the oxidation was dominated by the alkynyl ligand with the mixing of metal-centered contribution. The intense absorption bands of **82a**-**82c** in the range of 299-375 nm are ascribed to the IL π→π* transitions of the alkynyl and cyclometalated N^C^N ligands, whereas the low-energy absorption bands of **82a** and **82b** at around 426-506 nm are attributed to the ICT transitions of the D-A alkynyl ligands accompanied by the MLCT/LLCT transition. The memory device based on **82a** demonstrated WORM-type binary memory behavior with a relatively low operating voltage of 3.5 V, high ON/OFF ratio (> 10^5) as well as long retention time (> 10^4 s), which are comparable to the aforementioned devices based on Au(III)-containing complexes. This work provides the fabrication of memory device based on the electric switching effect, which is attributed to the CT process between the donor and acceptor moieties in Pt(II)-containing alkynyl complexes.

3.4. Chemo/biosensing

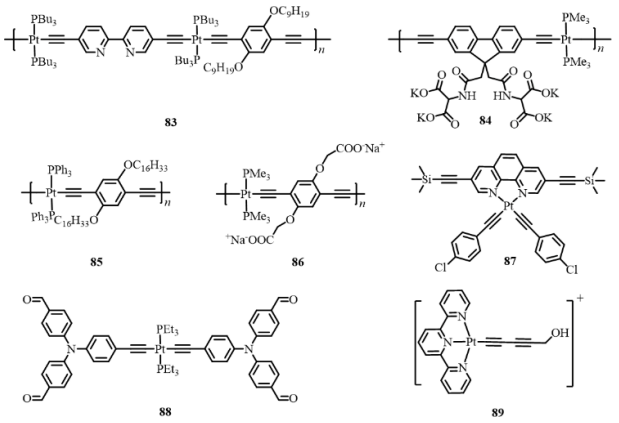

As important branches of organic electronics, numerous chemo/biosensing methods have been established to meet multiple detection requirements. Typically, chemo/biosensors consist of receptor units and signaling units, the former are responsible for binding the analytes selectively, while this specific interaction can be reflected by the latter through the changes in optical or other properties. Notably, these two parts can be incorporated into metallated complexes or conjugated polymers, providing a scalable platform for the construction of chemo/biosensors.

Pt(II)-acetylide polymer **83** was prepared as a chemosensor for the detection of metal cations, in which the 2,2'-bipyridine units in the backbone provide ideal transition metal ion binding sites in the sensing process.[78] In most cases, the metal ion-bipyridine complexation leads to the phosphorescence quenching in the polymer and the corresponding model complex. The addition of Cu^{2+} and Ni^{2+} results in a more efficient phosphorescence quenching in polymer as compared to its model complex, proving the amplified signal output effect of polymer **83** in the sensing process. Moreover,

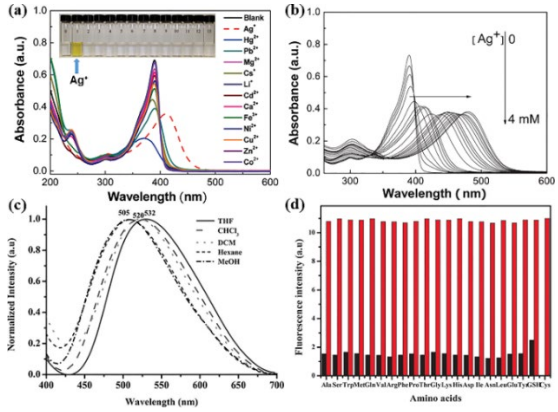

Figure 18 (a) Absorption spectra of polymer **84** in the presence of various metal ions in degassed water, [**84**] = 5×10^{-6} mol/L, [Metal ion] = 1×10^{-5} mol/L. The inset is the photograph illustrating the special color change of **84** in the presence of Ag^+ ions as compared with other representative metal ions. (b) Absorption spectral response of **84** upon the addition of Ag^+ ions, [**84**] = 5×10^{-6} mol/L. Reproduced with the permission from ref. 79. Copyright 2011, American Chemical Society. (c) Vapochromism of **88** after exposure to different solvent vapors. (d) Fluorescence responses of **88** towards cysteine in the presence of various amino acids after excitation at 310 nm. Black bars represent the fluorescence intensity of the solution of **88** after the addition of various amino acids. Red bars represent the fluorescence intensity of the solution upon further addition of cysteine. Reproduced with permission from ref. 82. Copyright 2016, Wiley-VCH.

the discrepant quenching capability of **83** for various metal ions is principally derived from the intrinsic quenching efficiency of different metal ion-bipyridine complexes with different association constants, laying a good foundation to semi-quantitative analysis.

Conjugated polyelectrolyte **84** containing the aspartic acid-substituted fluorene spacer was applied as a chemosensor, showing excellent water solubility, processability and ionic nature.[79] **84** demonstrated the intriguing fluorescent and phosphorescent dual emission in pure aqueous medium at room temperature. The sensor based on **84** can afford the direct colorimetric detection of Ag^+ ions in aqueous media with high selectivity and sensitivity, which is attributed to the introduction of electron-rich amino acid groups in the side chains and the ISC process induced by Ag^+. The addition of Ag^+ ions into the solution of **84** results in the increased phosphorescence intensity and decreased fluorescence intensity accompanied with the red shifts in their emission peaks. This Ag^+-responsive color change from colorless to yellow can be observed by naked eyes and detected quantitatively by absorption spectroscopy (Figure 18a and b).

The membrane of **85** was employed as a surface acoustic wave (SAW)-based sensor towards relative humidity and chemical vapors.[80] The films exhibited nanoscale columnar growth at a vertical edge of the cracked membrane in the scanning electron microscopy (SEM) observation. The exposure of the membrane of **85** to the detected analytes brings a change to the phase velocity of SAW, exhibiting a phase shift in the output electric signals of the electroacoustic device. This device demonstrated a satisfactory sensitivity in very low humidity conditions (relative humidity < 10%). Besides, polymer **85** is also sensitive to acetone and methanol, whereas the sensitivities of **85** towards these analytes are relatively lower than that for relative humidity. A pH sensor was developed based on Pt(II)-acetylide polyelectrolyte **86**, which displayed long-lived phosphorescence from the triplet ππ* excitons.[81] The significant changes in the photophysical properties of the prepared polymer during the sensing process are ascribed to the variation in the conformational states of **86** under different pH conditions. The carboxyl groups are protonated at low pH condition with the formation of polymer aggregates comprising face-to-face stacked chains, which leads to the blue shift in absorption spectra and the quenching of phosphorescence.

Complex **87** containing dual-recognition sites was fabricated for the detection of benzene vapor.[36] There are two host-guest recognition units in the square-planar structure: one is the H-bond site between two phenylacetylene ligands, another one is the π-π stacking site above the phenanthroline rings which provide strong π-π interactions with the aromatic analytes. By exposing **87** to different saturated volatile organic compound (VOC) vapors, it exhibited a high sensitivity towards benzene compounds by presenting a red color under ambient light. **87** also gave a red luminescence with the strong emission band centered at 634-654 nm under UV light irradiation. However, yellow color or the yellow luminescence was found in this system when **87** was treated with other VOCs, indicating its remarkable sensitivity towards benzene compounds.

Luminogen **88** was decorated with functional aldehyde units to promote its photophysical properties via donor-acceptor interaction.[82] The compound in ordered crystalline aggregates showed a stronger fluorescence in solution with a moderate water content (70%), while the increased water content resulted in the formation of amorphous aggregates accompanied by lower fluorescence intensity. Compound **88** and its analogue without Pt(II) ion both demonstrated crystallization-induced emission enhancement (CIEE) feature, and their crystalline states are more suitable to be utilized as emitters compared to their grinded

states. Such unique optical behavior is mainly derived from the weak intermolecular hydrogen bonding and C-H···π interactions in the crystalline states. As demonstrated in Figure 18c, different emission peak maxima were detected due to the exposure of **88** in various solvent vapors. This system also showed a high selectivity towards cysteine with a chemodosimetric response in physiological conditions (Figure 18d).

Pt(II)-containing terpyridyl complex **89** was employed for the effective detection of G-quadruplex and nuclease activity.[83] By using K^+ ions to stabilize the short G-rich oligonucleotides, **89** demonstrated self-assembly behavior via Pt(II)···Pt(II) and π-π interactions triggered by the formation of G-quadruplexes. The electrostatic interaction between the positively charged complex **89** and the negatively charged G-quadruplex provides a basis for such aggregation process. With the presence of oligonucleotide TGGG and the stabilizing ion K^+, the addition of **89** into the system leads to a new absorption band at around 550 nm as well as an emission band in the NIR region, indicating the successful self-assembly of **89**. Furthermore, the nuclease activity can be monitored by the spectral variation of **89**, which is also based on its self-assembly characteristics. This work can put forward a detection method towards both the formation of DNA G-quadruplex and nuclease activity without the labeling operation or the formation of covalent bonds between Pt(II)-containing complex and the oligonucleotides.

4. Conclusions and perspectives

In conclusion, the structures and properties of polymeric and molecular metallaynes containing platinum, mercury and gold are discussed in this perspective article with their optical, electronic and magnetic applications. Numerous acetylide-containing metallated polymers and molecules with specific functions have been developed through their rational design and deliberate chemical synthesis, which is closely linked to the in-depth exploration of the structure-property relationships in these compounds. The appropriate selection of metal centers, auxiliary ligands and organic spacers endows these organometallic systems with controllable properties, leading to their promising applications in energy conversion, nonlinear optics, data storage and memory, as well as chemo/biosensing. Among them, OLEDs and solar cells are two representative categories of optoelectronic devices for energy interconversion, whilst the emerging application of metallated polyynes as the OTE materials has also been exploited in recent years. These efficient energy conversion strategies are undoubtedly of great significance to circumvent the energy crisis in our society nowadays. Furthermore, the utilization of such metallated conjugated compounds in MRAM and RRAM devices has been explored successfully, thereby providing scalable approaches to meet the memory and data storage demands of the forthcoming Big Data era. Obviously, the research on functional acetylide-containing metallated compounds has consistently contributed to the developments in the optoelectronic and materials science fields.

Since the pivotal role of metal centers has been demonstrated in these Pt(II)-, Hg(II)-, Au(I)- and Au(III)-containing conjugated systems, the library of organometallic acetylide-containing compounds can be further expanded by deploying other transition metal blocks to acquire abundant molecular structures and diversified functions. Although polymeric and molecular metallaynes with group 8 metal centers have aroused extensive research attention in the past few years, there are relatively less reports focused on these compounds compared to their group 10 metal-based counterparts. It is worth noting that the photophysical properties and redox behaviors of such group 8 metal-based systems, especially of those with Fe(II) or Ru(II) centers, have been investigated to a certain extent, revealing their impressive potentials in related optoelectronic applications. By contrast, there are only limited reports on group 9 metal-based acetylide-containing compounds due to the low stability of these metal centers. However, these compounds exhibit intriguing photochemical properties which are different from their counterparts bearing other metal ions.[84] Furthermore, reports focused on various metallopolymers and metal-organic complexes provide valuable references and available synthetic strategies for the construction of organometallic systems bearing various metal elements.[85-90] Therefore, research endeavor still needs to be focused on the development of other novel organometallic systems to conquer the obstacles remained in this field. We believe that this research topic is essential to elucidate a comprehensive evaluation of the impact of different metal centers on the material properties and the structure-function-activity relationships in various metallic conjugated systems, thereby leading to their practical applications and commercial prospects in the greater context.

Evidently, the rapid development of these application-oriented organometallic polyynes is inextricably bound up with their devisable chemical structures and geometric configurations, which are both derived from the diversified synthetic methodologies. Encouraged by the successful explorations of rigid-rod 1D polymetallaynes, research attention has been turned to the multi-dimensional organometallic materials. In particular, the highly-ordered conjugated architectures in 2D organometallic materials contribute vastly to the remarkable stability and enhanced optoelectronic performance in these materials. Although graphynes have been developed as an emerging type of carbon-rich materials in recent years, the studies about metallated graphynes are still in an initial phase, where the limited areas and unsatisfactory film-forming properties hinder their practical applications. Our successful attempt in preparing Hg(II)-based graphyne nanosheets by the bottom-up method provides a unique perspective to address these issues. From the preliminary studies, this approach can also be applied to obtain the large-area nanosheets with other metal chromophores (for instance, the square-planar Pt(II) blocks). These results offer an enlightening paradigm for the fabrication of novel 2D metallated graphynes, in which the geometric configuration and macroscopic morphology can be regulated by adopting various metal building blocks and auxiliary ligands. Noteworthily, the synthetic variability allows the introduction of necessary heteroatoms as redox or active sites to such organometallic nano-frameworks, which can enormously broaden the potential applications of these 2D polymeric materials. According to our recent reports, ultrastable electroreduction of CO_2 to CO can be realized with the selectivity of nearly 100% by deploying metalloporphyrin-linked mercurated graphynes as the catalyst, whilst the combination of mercurated graphyne HgL1 and carbon quantum dots leads to high-efficiency photoinduced H_2O_2 production, indicating the bright application prospect of 2D metallated graphynes in the energy field.[91-92] Further investigation and refinement following this direction will definitely lead to an insightful comprehension of the fascinating optoelectronic behaviors and structure-property-function relationships in such multi-dimensional organometallic conjugated systems. It is foreseeable that considerable cutting-edge applications of such organometallic nanosheets will be developed by the persistently experimental and theoretical explorations in this field, which are attractive to both academic research and industrial exploitation.

Acknowledgement

W.Y.W. is grateful to the financial support from the Hong

Kong Research Grants Council (PolyU 15307321), the RGC Senior Research Fellowship Scheme (SRFS2021-5S01), the CAS-Croucher Funding Scheme for Joint Laboratories (ZH4A), the Guangdong-Hong Kong-Macao Joint Laboratory of Optoelectronic and Magnetic Functional Materials (2019B121205002), Research Institute for Smart Energy (CDAQ) and Miss Clarea Au for the Endowed Professorship in Energy (847S).

References

[1] Wong, W.-Y. Metallated Molecular Materials of Fluorene Derivatives and Their Analogues. *Coord. Chem. Rev.* **2005**, *249*, 971—997.

[2] Zhao, X.; Zhan, X. Electron Transporting Semiconducting Polymers in Organic Electronics. *Chem. Soc. Rev.* **2011**, *40*, 3728—3743.

[3] Ho, C.-L., Yu, Z., Wong, W.-Y. Multifunctional Polymetallaynes: Properties, Functions and Applications. *Chem. Soc. Rev.* **2016**, *45*, 5264—5295.

[4] Whittell, G. R.; Hager, M. D.; Schubert, U. S.; Manners, I. Functional Soft Materials from Metallopolymers and Metallosupramolecular Polymers. *Nat. Mater.* **2011**, *10*, 176—188.

[5] Wong, W.-Y.; Ho, C.-L. Di-, Oligo- and Polymetallaynes: Syntheses, Photophysics, Structures and Applications. *Coord. Chem. Rev.* **2006**, *250*, 2627—2690.

[6] Fujikura, Y.; Sonogashira, K.; Hagihara, N. Preparation and UV Spectra of Some Oligomer-Complexes Composed of Platinum Group Metals and Conjugated Poly-yne Systems. *Chem. Lett.* **1975**, 1067—1070.

[7] Sonogashira, K.; Takahashi, S.; Hagihara, N. A New Extended Chain Polymer. Poly[*trans*-bis(tri-*n*-butylphosphine)platinum 1,4-butadiynediyl]. *Macromolecules* **1977**, *10*, 879—880.

[8] Xu, L.; Sun, J.; Tang, T.; Zhang, H.; Sun, M.; Zhang, J.; Li, J.; Huang, B.; Wang, Z.; Xie, Z.; Wong, W.-Y. Metallated Graphynes as a New Class of Photofunctional 2D Organometallic Nanosheets. *Angew. Chem. Int. Ed.* **2021**, *60*, 11326—11334.

[9] Zhang, J.; Xu, L.; Ho, C.-L.; Wong, W.-Y. Functional Organometallic Poly(arylene ethynylene)s: From Synthesis to Applications. *Top Curr. Chem.* **2017**, *375*, 77.

[10] Liu, L.; Poon, S.-Y.; Wong, W.-Y. Evolution of Lowest Singlet and Triplet Excited States with Transition Metals in Group 10-12 Metallaynes Containing Biphenyl Spacer. *J. Organomet. Chem.* **2005**, *690*, 5036—5048.

[11] Guo, F.; Kim, Y.-G.; Reynolds, J. R.; Schanze, K. S. Platinum-Acetylide Polymer Based Solar Cells: Involvement of the Triplet State for Energy Conversion. *Chem. Commun.* **2006**, 1887—1889.

[12] Chawdhury, N.; Köhler, A.; Friend, R. H.; Wong, W.-Y.; Lewis, J.; Younus, M.; Raithby, P. R.; Corcoran, T. C.; Al-Mandhary, M. R. A.; Khan, M. S. Evolution of Lowest Singlet and Triplet Excited States with Number of Thienyl Rings in Platinum Poly-ynes. *J. Chem. Phys.* **1999**, *110*, 4963—4970.

[13] Khan, M. S.; Al-Mandhary, M. R. A.; Al-Suti, M. K.; Al-Battashi, F. R.; Al-Saadi, S.; Ahrens, B.; Bjernemose, J. K.; Mahon, M. F.; Raithby, P. R.; Younus, M.; Chawdhury, N.; Köhler, A.; Marseglia, E. A.; Tedesco, E.; Feeder, N.; Teat, S. J. Synthesis, Characterisation and Optical Spectroscopy of Platinum(II) Di-ynes and Poly-ynes Incorporating Condensed Aromatic Spacers in the Backbone. *Dalton Trans.* **2004**, 2377—2385.

[14] Devi, L. S.; Al-Suti, M. K.; Zhang, N.; Teat, S. J.; Male, L.; Sparkes, H. A.; Raithby, P. R.; Khan, M. S.; Köhler, A. Synthesis and Comparison of the Optical Properties of Platinum(II) Poly-ynes with Fused and Non-Fused Oligothiophenes. *Macromolecules* **2009**, *42*, 1131—1141.

[15] Markwell, R. D.; Butler, I. S.; Kakkar, A. K.; Khan, M. S.; Al-Zakwani, Z. H.; Lewis, J. Vibrational Spectroscopic Investigation of Rigid-Rod Platinum α-Acetylide Polymers Containing Variable Acetylenic Microstructures. *Organometallics* **1996**, *15*, 2331—2337.

[16] Wilson, J. S.; Chawdhury, N.; Al-Mandhary, M. R. A.; Younus, M.; Khan, M. S.; Raithby, P. R.; Köhler, A.; Friend, R. H. The Energy Gap Law for Triplet States in Pt-Containing Conjugated Polymers and Monomers. *J. Am. Chem. Soc.* **2001**, *123*, 9412—9417.

[17] Wong, W.-Y.; Wong, C.-K.; Lu, G.-L.; Lee, A. W.-M.; Cheah, K.-W.; Shi, J.-X. Triplet Emission in Platinum-Containing Poly(alkynylsilanes). *Macromolecules* **2003**, *36*, 983—990.

[18] Wong, W.-Y.; Liu, L.; Poon, S.-Y.; Choi, K.-H.; Cheah, K.-W.; Shi, J.-X. Harvesting of Organic Triplet Emissions in Metal Diynes and Polyynes of Group 10-12 Transition Elements Containing the Conjugation-Interrupting Diphenylfluorene Unit. *Macromolecules* **2004**, *37*, 4496—4504.

[19] Liu, L.; Wong, W.-Y.; Shi, J.-X.; Cheah, K.-W.; Lee, T.-H.; Leung, L. M. Synthesis, Spectroscopy, Structures and Photophysics of Metal Alkynyl Complexes and Polymers Containing Functionalized Carbazole Spacers. *J. Organomet. Chem.* **2006**, *691*, 4028—4041.

[20] Wong, W.-Y.; Wong, C.-K.; Lu, G.-L.; Cheah, K.-W.; Shi, J.-X.; Lin, Z. Synthesis, Structures and Optical Spectroscopy of Photoluminescent Platinum-Linked Poly(silylacetylenes). *J. Chem. Soc., Dalton Trans.* **2002**, 4587—4594.

[21] Wong, W.-Y.; Poon, S.-Y.; Lee, A. W.-M.; Shi, J.-X.; Cheah, K.-W. Oligo(fluorenyleneethynylenegermylene)s and Their Metallopolymers. *Chem. Commun.* **2004**, 2420—2421.

[22] Wong, W.-Y.; Poon, S.-Y.; Shi, J.-X.; Cheah, K.-W. Synthesis, Optical Properties, and Photoluminescence of Organometallic Acetylide Polymers of Platinum Functionalized with Si and Ge-Bridged Bis(3,6-diethynyl-9-butylcarbazole). *J. Inorg. Organomet. P.* **2007**, *17*, 189—200.

[23] Poon, S.-Y.; Wong, W.-Y.; Cheah, K.-W.; Shi, J.-X. Spatial Extent of the Singlet and Triplet Excitons in Luminescent Angular-Shaped Transition-Metal Diynes and Polyynes Comprising Non-π-Conjugated Group 16 Main Group Elements. *Chem. Eur. J.* **2006**, *12*, 2550—2563.

[24] Wang, Q.; He, Z.; Wild, A.; Wu, H.; Cao, Y.; Schubert, U. S.; Chui, C.-H.; Wong, W.-Y. Platinum-Acetylide Polymers with Higher Dimensionality for Organic Solar Cells. *Chem. Asian J.* **2011**, *6*, 1766—1777.

[25] Wong, W.-Y. Mercury Alkynyls as Versatile Templates for New Organometallic Materials and Polymers. *Coord. Chem. Rev.* **2007**, *251*, 2400—2427.

[26] Liu, L.; Li, M.-X.; Wong, W.-Y. Synthesis and Luminescent Properties of Mercury(II) Polyynes Containing Derivatized Benzene in the Backbone. *Aust. J. Chem.* **2005**, *58*, 799—802.

[27] Wong, W.-Y.; Liu, L.; Shi, J.-X. Triplet Emission in Soluble Mercury(II) Polyyne Polymers. *Angew. Chem. Int. Ed.* **2003**, *42*, 4064—4068.

[28] Irwin, M. J.; Vittal, J. J.; Puddephatt, R. J. Luminescent Gold(I) Acetylides: From Model Compounds to Polymers. *Organometallics* **1997**, *16*, 3541—3547.

[29] Li, L.; Ho, C.-L.; Wong, W.-Y. Versatile Control of the Optical Bandgap in Heterobimetallic Polymers through Complexation of Bithiazole-Containing Polyplatinynes with $ReCl(CO)_5$. *J. Organomet. Chem.* **2012**, *703*, 43—50.

[30] Dong, Q.; Qu, W.; Liang, W.; Guo, K.; Xue, H.; Guo, Y.; Meng, Z.; Ho, C.-L.; Leung, C.-W.; Wong, W.-Y. Metallopolymer Precursors to $L1_0$-CoPt Nanoparticles: Synthesis, Characterization, Nanopatterning and Potential Application. *Nanoscale* **2016**, *8*, 7068—7074.

[31] Zhou, G.-J.; Wong, W.-Y.; Ye, C.; Lin, Z. Optical Power Limiters Based on Colorless Di-, Oligo-, and Polymetallaynes: Highly Transparent Materials for Eye Protection Devices. *Adv. Funct. Mater.* **2007**, *17*, 963—975.

[32] Ho, C.-L.; Chui, C.-H.; Wong, W.-Y.; Aly, S. M.; Fortin, D.; Harvey, P. D.; Yao, B.; Xie, Z.; Wang, L. Efficient Electrophosphorescence from a Platinum Metallopolyyne Featuring a 2,7-Carbazole Chromophore. *Macromol. Chem. Phys.* **2009**, *210*, 1786—1798.

[33] Wong, W. Y.; Zhou, G. J.; He, Z.; Cheung, K. Y.; Ng, A. M. C.; Djurišić, A. B.; Chan, W. K. Organometallic Polymer Light-Emitting Diodes Derived from a Platinum(II) Polyyne Containing the Bithiazole Ring. *Macromol. Chem. Phys.* **2008**, *209*, 1319—1332.

[34] Goudreault, T.; He, Z.; Guo, Y.; Ho, C.-L.; Zhan, H.; Wang, Q.; Ho, K. Y.-F.; Wong, K.-L.; Fortin, D.; Yao, B.; Xie, Z.; Wang, L.; Kwok, W.-M.; Harvey, P. D.; Wong, W.-Y. Synthesis, Light-Emitting, and Two-Photon Absorption Properties of Platinum-Containing Poly(arylene-ethynylene)s Linked by 1,3,4-Oxadiazole Units. *Macromolecules* **2010**, *43*, 7936—7949.

[35] Zhou, G.; He, Y.; Yao, B.; Dang, J.; Wong, W.-Y.; Xie, Z.; Zhao, X.; Wang, L. Electrophosphorescent Heterobimetallic Oligometallaynes and Their Applications in Solution-Processed Organic Light-Emitting Devices. *Chem. Asian J.* **2010**, *5*, 2405—2414.

[36] Huang, Z.; Liu, B.; Zhao, J.; He, Y.; Yan, X.; Xu, X.; Zhou, G.; Yang, X.; Wu, Z. Platinum(II) Polymetallayne-Based Phosphorescent Polymers with Enhanced Triplet Energy-Transfer: Synthesis, Photophysical, Electrochemistry, and Electrophosphorescent Investigation. *RSC Adv.* **2015**, *5*, 36507—36519.

[37] Chang, Y.-C.; Tang, K.-C.; Pan, H.-A.; Liu, S.-H.; Koshevoy, I. O.; Karttunen, A. J.; Hung, W.-Y.; Cheng, M.-H.; Chou, P.-T. Harnessing Fluorescence Versus Phosphorescence Branching Ratio in $(Phenyl)_n$-Bridged (n = 0-5) Bimetallic Au(I) Complexes. *J. Phys. Chem. C* **2013**, *117*, 9623—9632.

[38] Wong, W.-Y. Challenges in Organometallic Research - Great Opportunity for Solar Cells and OLEDs. *J. Organomet. Chem.* **2009**, *694*, 2644—2647.

[39] Whittell, G. R.; Hager, M. D.; Schubert, U. S.; Manners, I. Functional Soft Materials from Metallopolymers and Metallosupramolecular Polymers. *Nat. Mater.* **2011**, *10*, 176—188.

[40] Xu, L.; Ho, C.-L.; Liu, L.; Wong, W.-Y. Molecular/Polymeric Metallaynes and Related Molecules: Solar Cell Materials and Devices. *Coord. Chem. Rev.* **2018**, *373*, 233—257.

[41] Wong, W.-Y.; Wang, X.-Z.; He, Z.; Djurišić, A. B.; Yip, C.-T.; Cheung, K.-Y.; Wang, H.; Mak, C. S. K.; Chan, W.-K. Metallated Conjugated Polymers as a New Avenue Towards High-Efficiency Polymer Solar Cells. *Nat. Mater.* **2007**, *6*, 521—527.

[42] Baek, N. S.; Hau, S. K.; Yip, H.-L.; Acton, O.; Chen, K.-S.; Jen, A. K.-Y. High Performance Amorphous Metallated π-Conjugated Polymers for Field-Effect Transistors and Polymer Solar Cells. *Chem. Mater.* **2008**, *20*, 5734—5736.

[43] Wong, W.-Y.; Wang, X.-Z.; He, Z.; Chan, K.-K.; Djurišić, A. B.; Cheung, K.-Y.; Yip, C.-T.; Ng, A. M.-C.; Xi, Y. Y.; Mak, C. S. K.; Chan, W.-K. Tuning the Absorption, Charge Transport Properties, and Solar Cell Efficiency with the Number of Thienyl Rings in Platinum-Containing Poly(aryleneethynylene)s. *J. Am. Chem. Soc.* **2007**, *129*, 14372—14380.

[44] Liu, L.; Ho, C.-L.; Wong, W.-Y.; Cheung, K.-Y.; Fung, M.-K.; Lam, W.-T.; Djurišić, A. B.; Chan, W.-K. Effect of Oligothienyl Chain Length on Tuning the Solar Cell Performance in Fluorene-Based Polyplatinynes. *Adv. Funct. Mater.* **2008**, *18*, 2824—2833.

[45] Dai, F.-R.; Zhan, H.-M.; Liu, Q.; Fu, Y.-Y.; Li, J.-H.; Wang, Q.-W.; Xie, Z.; Wang, L.; Yan, F.; Wong, W.-Y. Platinum(II)-Bis(aryleneethynylene) Complexes for Solution-Processible Molecular Bulk Heterojunction Solar Cells. *Chem. Eur. J.* **2012**, *18*, 1502—1511.

[46] He, W.; Livshits, M. Y.; Dickie, D. A.; Zhang, Z.; Mejiaortega, L. E.; Rack, J. J.; Wu, Q.; Qin, Y. "Roller-Wheel"-Type Pt-Containing Small Molecules and the Impact of "Rollers" on Material Crystallinity, Electronic Properties, and Solar Cell Performance. *J. Am. Chem. Soc.* **2017**, *139*, 14109—14119.

[47] Dai, F.-R.; Chen, Y.-C.; Lai, L.-F.; Wu, W.-J.; Cui, C.-H.; Tan, G.-P.; Wang, X.-Z.; Lin, J.-T.; Tian, H.; Wong, W.-Y. Unsymmetric Platinum(II) Bis(aryleneethynylene) Complexes as Photosensitizers for Dye-Sensitized Solar Cells. *Chem. Asian J.* **2012**, *7*, 1426—1434.

[48] Ho, C.-L.; Wong, W.-Y. High Performance Arylamine-Based Metallated and Metal-Free Organic Photosensitizers for Dye-Sensitized Solar Cells. *J. Photoch. Photobio. C: Photoch. Rev.* **2016**, *28*, 138—158.

[49] Housecroft, C. E.; Constable, E. C. The Emergence of Copper(I)-Based Dye Sensitized Solar Cells. *Chem. Soc. Rev.* **2015**, *44*, 8386—8398.

[50] Bomben, P. G.; Robson, K. C. D.; Koivisto, B. D.; Berlinguette, C. P. Cyclometalated Ruthenium Chromophores for the Dye-Sensitized Solar Cell. *Coord. Chem. Rev.* **2012**, *256*, 1438—1450.

[51] Hagfeldt, A.; Boschloo, G.; Sun, L.; Kloo, L.; Pettersson, H. Dye-Sensitized Solar Cells. *Chem. Rev.* **2010**, *110*, 6595—6663.

[52] Zhang, S.; Yang, X.; Numata, Y.; Han, L. Highly Efficient Dye-Sensitized Solar Cells: Progress and Future Challenges. *Energy Environ. Sci.* **2013**, *6*, 1443—1464.

[53] Siu, C. H.; Lee, L. T.; Yiu, S. C.; Ho, P. Y.; Zhou, P.; Ho, C. L.; Chen, T.; Liu, J.; Han, K.; Wong, W. Y. Synthesis and Characterization of Phenothiazine-Based Platinum(II)-Acetylide Photosensitizers for Efficient Dye-Sensitized Solar Cells. *Chem. Eur. J.* **2016**, *22*, 3750—3757.

[54] Sun, Z.; Li, J.; Wong, W. Y. Emerging Organic Thermoelectric Applications from Conducting Metallopolymers. *Macromol. Chem. Phys.* **2020**, *221*, 2000115.

[55] Wan, T.; Yin, X.; Pan, C.; Liu, D.; Zhou, X.; Gao, C.; Wong, W.-Y.; Wang, L. Boosting the Adhesivity of π-Conjugated Polymers by Embedding Platinum Acetylides Towards High-Performance Thermoelectric Composites. *Polymers* **2019**, *11*, 593—607.

[56] Yin, X.; Wan, T.; Deng, X.; Xie, Y.; Gao, C.; Zhong, C.; Xu, Z.; Pan, C.; Chen, G.; Wong, W.-Y.; Yang, C.; Wang, L. De Novo Design of Polymers Embedded with Platinum Acetylides Towards n-Type Organic Thermoelectrics. *Chem. Eng. J.* **2021**, *405*, 126692.

[57] Zhou, G.-J.; Wong, W.-Y. Organometallic Acetylides of Pt(II), Au(I) and Hg(II) as New Generation Optical Power Limiting Materials. *Chem. Soc. Rev.* **2011**, *40*, 2541—2566.

[58] Zhou, G.-J.; Wong, W.-Y.; Cui, D.; Ye, C. Large Optical-Limiting Response in Some Solution-Processable Polyplatinaynes. *Chem. Mater.* **2005**, *17*, 5209—5217.

[59] Zhou, G.-J.; Wong, W.-Y.; Lin, Z.; Ye, C. White Metallopolyynes for Optical Limiting/Transparency Trade-Off Optimization. *Angew. Chem. Int. Ed.* **2006**, *45*, 6189—6193.

[60] Tian, Z.; Yang, X.; Liu, B.; Zhao, J.; Zhong, D.; Wu, Y.; Zhou, G.; Wong, W.-Y. Novel Au^{I} Polyynes and Their High Optical Power Limiting Performances Both in Solution and in Prototype Devices. *J. Mater. Chem. C* **2018**, *6*, 6023—6032.

[61] Zhou, G.; Wong, W.-Y.; Poon, S.-Y.; Ye, C.; Lin, Z. Symmetric Versus Unsymmetric Platinum(II) Bis(aryleneethynylene)s with Distinct Electronic Structures for Optical Power Limiting/Optical Transparency Trade-Off Optimization. *Adv. Funct. Mater.* **2009**, *19*, 531—544.

[62] Liu, B.; Tian, Z.; Dang, F.; Zhao, J.; Yan, X.; Xu, X.; Yang, X.; Zhou, G.; Wu, Y. Photophysical and Optical Power Limiting Behaviors of Au(I) Acetylides with Diethynyl Aromatic Ligands Showing Different Electronic Features. *J. Organomet. Chem.* **2016**, *804*, 80—86.

[63] Lian, H.; Cheng, X.; Hao, H.; Han, J.; Lau, M.-T.; Li, Z.; Zhou, Z.; Dong, Q.; Wong, W.-Y. Metal-Containing Organic Compounds for Memory and Data Storage Applications. *Chem. Soc. Rev.* **2022**, *51*, 1926—1982.

[64] Wang, Y.; Astruc, D.; Abd-El-Aziz, A. S. Metallopolymers for Advanced Sustainable Applications. *Chem. Soc. Rev.* **2019**, *48*, 558—636.

[65] Streubel, R.; Fischer, P.; Kronast, F.; Kravchuk, V. P.; Sheka, D. D.; Gaididei, Y.; Schmidt, O. G.; Makarov, D. Magnetism in Curved Geometries. *J. Phys. D: Appl. Phys.* **2016**, *49*, 363001.

[66] Dong, Q.; Li, G.; Ho, C.-L.; Faisal, M.; Leung, C.-W.; Pong, P. W.-T.; Liu, K.; Tang, B.-Z.; Manners, I.; Wong, W.-Y. A Polyferroplatinyne Precursor for the Rapid Fabrication of $L1_0$-FePt-Type Bit Patterned Media by Nanoimprint Lithography. *Adv. Mater.* **2012**, *24*, 1034—1040.

[67] Salahuddin, S.; Ni, K.; Datta, S. The Era of Hyper-Scaling in Electronics. *Nat. Electron.* **2018**, *1*, 442—450.

[68] Liu, K.; Ho, C.-L.; Aouba, S.; Zhao, Y.-Q.; Lu, Z.-H.; Petrov, S.; Coombs, N.; Dube, P.; Ruda, H. E.; Wong, W.-Y.; Manners, I. Synthesis and Lithographic Patterning of FePt Nanoparticles Using a Bimetallic Metallopolyyne Precursor. *Angew. Chem. Int. Ed.* **2008**, *47*, 1255—1259.

[69] Dong, Q.; Li, G.; Wang, H.; Pong, P. W.-T.; Leung, C.-W.; Manners, I.; Ho, C.-L.; Li, H.; Wong, W.-Y. Investigation of Pyrolysis Temperature in the One-Step Synthesis of $L1_0$ FePt Nanoparticles from a FePt-Containing Metallopolymer. *J. Mater. Chem. C* **2015**, *3*, 734—741.

[70] Kim, J.; Rong, C.; Liu, J. P.; Sun, S. Dispersible Ferromagnetic FePt Nanoparticles. *Adv. Mater.* **2009**, *21*, 906—909.

[71] Meng, Z.; Li, G.; Wong, H.-F.; Ng, S.-M.; Yiu, S.-C.; Ho, C.-L.; Leung, C.-W.; Manners, I.; Wong, W.-Y. Patterning of $L1_0$ FePt Nanoparticles with Ultra-High Coercivity for Bit-Patterned Media. *Nanoscale* **2017**, *9*, 731—738.

[72] Meng, Z.; Li, G.; Ng, S.-M.; Wong, H.-F.; Yiu, S.-C.; Ho, C.-L.; Leung, C.-W.; Wong, W.-Y. Nanopatterned $L1_0$-FePt Nanoparticles from Single-Source Metallopolymer Precursors for Potential Application in Ferromagnetic Bit-Patterned Media Magnetic Recording. *Polym. Chem.* **2016**, *7*, 4467—4475.

[73] Meng, Z.; Wei, Z.; Fu, K.; Lv, L.; Yu, Z.-Q.; Wong, W.-Y. Amphiphilic Bimetallic Polymer as Single-Source Precursors for the One-Pot Synthesis of $L1_0$-Phase FePt Nanoparticles. *J. Organomet. Chem.* **2019**, *892*, 83—88.

[74] Meng, Z.; Ho, C.-L.; Wong, H.-F.; Yu, Z.-Q.; Zhu, N.; Li, G.; Leung, C.-W.; Wong, W.-Y. Lithographic Patterning of Ferromagnetic FePt Nanoparticles from a Single-Source Bimetallic Precursor Containing Hemiphasmidic Structure for Magnetic Data Recording Media. *Sci. China Mater.* **2018**, *62*, 566—576.

[75] Au, V. K.-M.; Wu, D.; Yam, V. W.-W. Organic Memory Devices Based on a Bis-Cyclometalated Alkynyl gold(III) Complex. *J. Am. Chem. Soc.* **2015**, *137*, 4654—4657.

[76] Hong, E. Y.-H.; Poon, C.-T.; Yam, V. W.-W. A Phosphole Oxide-Containing Organogold(III) Complex for Solution-Processable Resistive Memory Devices with Ternary Memory Performances. *J. Am. Chem. Soc.* **2016**, *138*, 6368—6371.

[77] Chan, A. K.-W.; Ng, M.; Wong, Y.-C.; Chan, M.-Y.; Wong, W.-T.; Yam, V. W.-W. Synthesis and Characterization of Luminescent Cyclometalated Platinum(II) Complexes with Tunable Emissive Colors and Studies of Their Application in Organic Memories and Organic Light-Emitting Devices. *J. Am. Chem. Soc.* **2017**, *139*, 10750—10761.

[78] Ogawa, K.; Guo, F.; Schanze, K. S. Phosphorescence Quenching of a Platinum Acetylide Polymer by Transition Metal Ions. *J. Photoch. Photobio. A: Chem.* **2009**, *207*, 79—85.

[79] Qin, C.; Wong, W.-Y.; Wang, L. A Water-Soluble Organometallic Conjugated Polyelectrolyte for the Direct Colorimetric Detection of Silver Ion in Aqueous Media with High Selectivity and Sensitivity. *Macromolecules* **2010**, *44*, 483—489.

[80] Caliendo, C.; Fratoddi, I.; Russo, M. V. Sensitivity of a Platinum-Polyyne-Based Sensor to Low Relative Humidity and Chemical Vapors. *Appl. Phys. Lett.* **2002**, *80*, 4849—4851.

[81] Haskins-Glusac, K.; Pinto, M. R.; Tan, C.; Schanze, K. S. Luminescence Quenching of a Phosphorescent Conjugated Polyelectrolyte. *J. Am. Chem. Soc.* **2004**, *126*, 14964—14971.

[82] Chowdhury, A.; Howlader, P.; Mukherjee, P. S. Mechano-Fluorochromic Pt(II) Luminogen and Its Cysteine Recognition. *Chem. Eur. J.* **2016**, *22*, 1424—1434.

[83] Yu, C.; Chan, K. H.-Y.; Wong, K. M.-C.; Yam, V. W.-W. Nucleic Acid-Induced Self-Assembly of a Platinum(II) Terpyridyl Complex: Detection of G-Quadruplex Formation and Nuclease Activity. *Chem. Commun.* **2009**, 3756—3758.

[84] Haque, A.; Al-Balushi, R. A.; Al-Busaidi, I. J.; Khan, M. S.; Raithby, P. R. Rise of Conjugated Poly-ynes and Poly(Metalla-ynes): From DesignThrough Synthesis to Structure-Property Relationships and Applications. *Chem. Rev.* **2018**, *118*, 8474—8597.

[85] Liu, X.; Yu, Z.; Yu, M.; Zhang, X.; Xu, Y.; Lv, P.; Chu, S.; Liu, C.; Lai, W.-Y.; Huang, W. Iridium(III)-Complexed Polydendrimers for Inkjet-Printing OLEDs: The Influence of Solubilizing Steric Hindrance Groups. *ACS Appl. Mater. Interfaces* **2019**, *11*, 26174—26184.

[86] Xu, H.; Chen, R.; Sun, Q.; Lai, W.; Su, Q.; Huang, W.; Liu, X. Recent Progress in Metal-Organic Complexes for Optoelectronic Applications. *Chem. Soc. Rev.* **2014**, *43*, 3259—3302.

[87] Lai, W.-Y.; Balfour, M. N.; Levell, J. W.; Bansal, A. K.; Burn, P. L.; Lo, S.-C.; Samuel, I. D. W. Poly(dendrimers) with Phosphorescent Iridium(III) Complex-Based Side Chains Prepared via Ring-Opening Metathesis Polymerization. *Macromolecules* **2012**, *45*, 2963—2971.

[88] Zhang, H.; Sun, Y.; Chen, Z.; Wang, W.; Wang, Q.; Chen, S.; Xu, Y.; Wong, W.-Y. Efficient Deep Red and NIR OLEDs based on Ir(III) Complexes Fabricated by Evaporation and Solution Processing. *Chem. Eng. J.* **2023**, *451*, 138632.

[89] Tao, P.; Lü, X.; Zhou, G.; Wong, W.-Y. Asymmetric Tris-Heteroleptic Cyclometalated Phosphorescent Iridium(III) Complexes: An Emerging Class of Metallophosphors. *Acc. Mater. Res.* **2022**, *3*, 830—842.

[90] Li, J.; Chen, K.; Wei, J.; Ma, Y.; Zhou, R.; Liu, S.; Zhao, Q.; Wong, W.-Y. Reversible On-Off Switching of Excitation-Wavelength-Dependent Emission of a Phosphorescent Soft Salt Based on Platinum(II) Complexes. *J. Am. Chem. Soc.* **2021**, *143*, 18317—18324.

[91] Fang, M.; Xu, L.; Zhang, H.; Zhu, Y.; Wong, W.-Y. Metalloporphyrin-Linked Mercurated Graphynes for Ultrastable CO_2 Electroreduction to CO with Nearly 100% Selectivity at a Current Density of 1.2 A cm^{-2}. *J. Am. Chem. Soc.* **2022**, *144*, 15143—15154.

[92] Zhao, Y.; Xu, L.; Wang, X.; Wang, Z.; Liu, Y.; Wang, Y.; Wang, Q.; Wang, Z.; Huang, H.; Liu, Y.; Wong, W.-Y.; Kang, Z. A Comprehensive Understanding on the Roles of Carbon Dots in Metallated Graphyne based Catalyst for Photoinduced H_2O_2 Production. *Nano Today* **2022**, *43*, 101428.